

Session 5. Plasma-wall interaction, propellants



**ExB Plasmas
Workshop
2022**

Madrid, online event

Universidad Carlos III de Madrid, February 16-18, 2022

Introduction

- I. Kaganovich et al. 'Physics of ExB discharges relevant to plasma propulsion and similar technologies' Phys. Plasmas 27, 120601 (2020), 11 sections
- **Section 2: Plasma–wall interaction in ExB discharges relevant to plasma propulsion devices**
- Current and future challenges / Advances in science and technology to meet them
 - SEE: to validate modeling predictions by comparison with measurements of electron VDF/EDF
 - Development of optical diagnostics (LTS,...), to achieve both short time and space resolution,
 - Development electrostatic diagnostics suitable for measurements of EEDF
 - A correct evaluation of the EVDF, in order to appropriately quantify the SEE effects
 - New sheaths models that account for non-Maxwellian EVDF
 - Oblique magnetic field adds considerable complexity, in the form of (not yet explored) magnetic striations.
 - Understand mutual interaction of turbulence and plasma–wall effects: turbulence leads to electron heating and scattering and can populate EVDF
 - How changes in the material properties by exposure to plasma affect the thruster operation
 - Research efforts in materials science to improve the performances of dielectric walls must continue
 - Research in designs minimizing relevance of plasma–wall effects: magnetically-shielded & wall-less thrusters

Contributions

- Eremin, Taccogna SEE modeling
- Cichocki Interaction of heavy species with walls
- Raitses Active boundaries for ExB plasmas
- Marín Kinetic modeling of electron-wall interaction
- Keidar Periodic structures in a magnetic field
- Polk Pole erosion characterization
- Mikellides Erosion and ion heating in MS-HETs
- Perales Plasma-wall simulations in MS-HETs
- Andreussi MS-HET scaling laws
- Taccogna Krypton vs xenon
- Rafalskyi Molecular propellant
Iodine

D. Eremin, F. Taccogna

Secondary Electron Emission Models

D. Eremin, Secondary Electron Emission Models in PIC

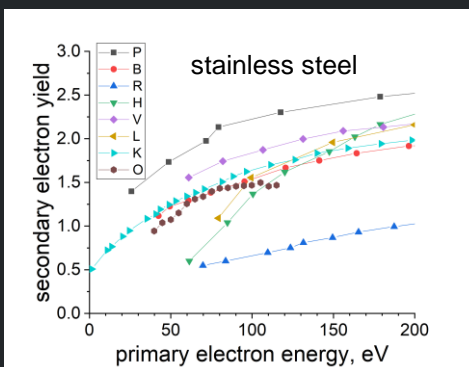
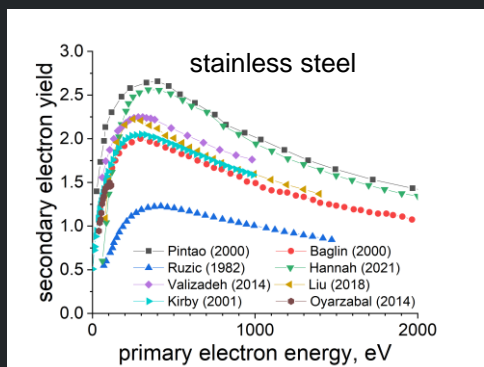
- **Secondary electron emission (SEE) is important:**

Affects power absorption, radial sheath physics, near-wall conductivity, couples with instabilities, etc.

- **Emitted electrons can be divided in 3 groups:**

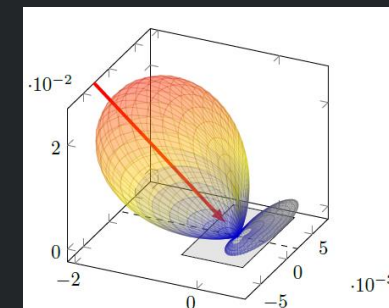
$$\delta = \delta_{ts} + \delta_r + \delta_e \quad (\text{true secondaries, "rediffused" aka inelastically backscattered, elastically reflected})$$

- **SEE Model should specify the yield, angular, and energy distributions**

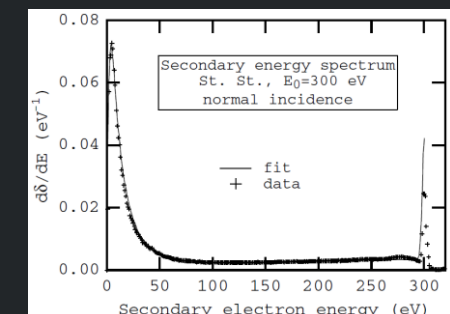


Ambiguity of experimental data on the SEE yield

- **Angular and energy distributions are important:** affect chemistry, penetration of the opposite sheath and yield at the opposite electrode, mirror reflections, etc.



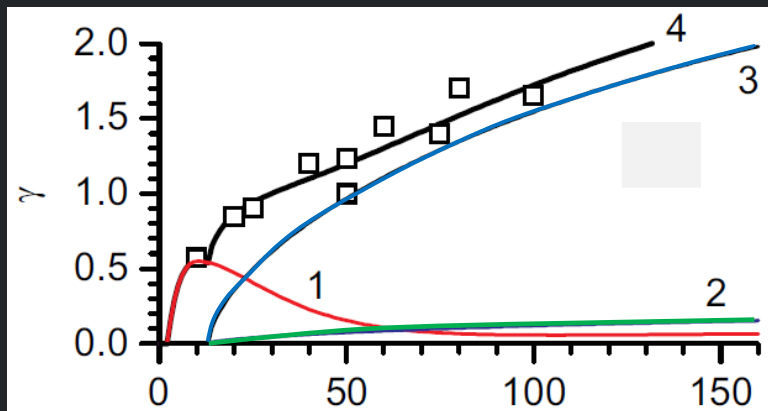
[Villemant et al., 2017]



[Furman and Pivi, 2002]

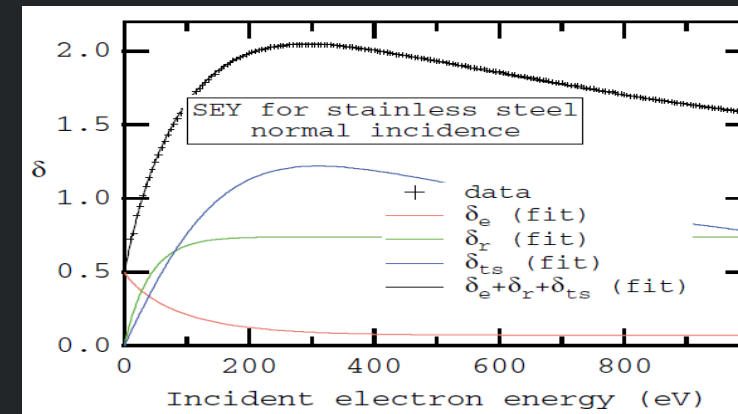
D. Eremin, Secondary Electron Emission Models in PIC

- Modified Vaughan's model (D. Sydorenko)



- 9 parameters for the yield, $\delta_r = C\delta_{ts}$. Low energy behavior is approximated by a “bumped” curve going to zero for small energies.
- Uniform energy distributions for the “e” and “r” electrons, half-Maxwellian for the “ts” electrons.

- Furman & Pivi

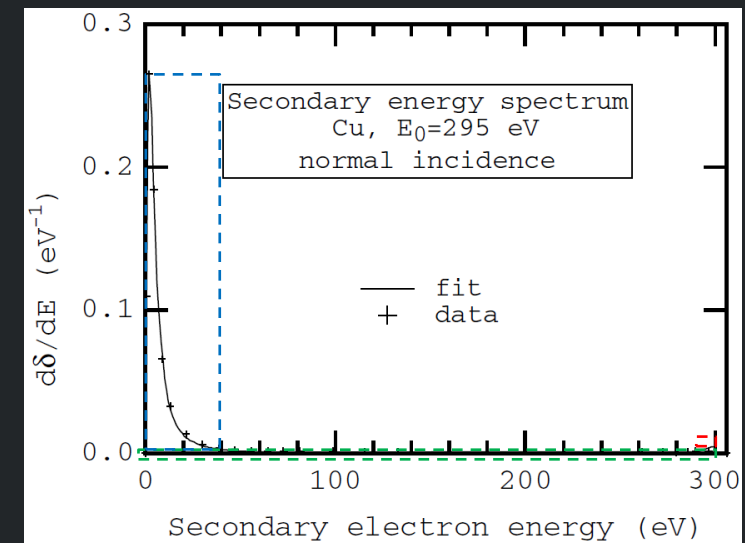
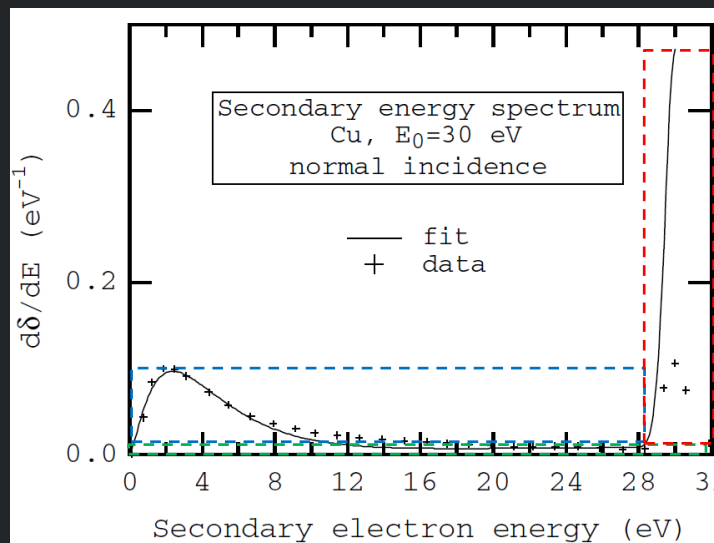
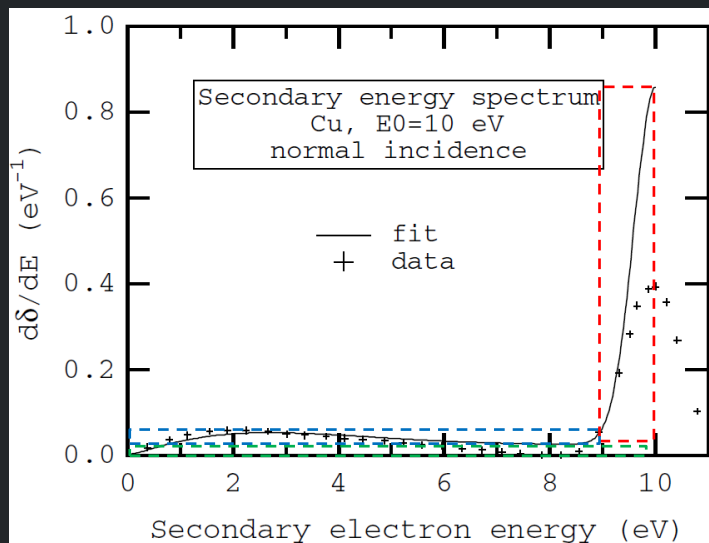


- 22 parameters for the yield, all groups have independent behavior. At low energies a finite coefficient for the elastically reflected electrons is assumed.
- An individual fitting formula for the energy distribution function of each group along with the corresponding Monte-Carlo procedure is suggested.

Different behavior of δ at low impact energies and different energy distributions!

D. Eremin, Secondary Electron Emission Models in PIC

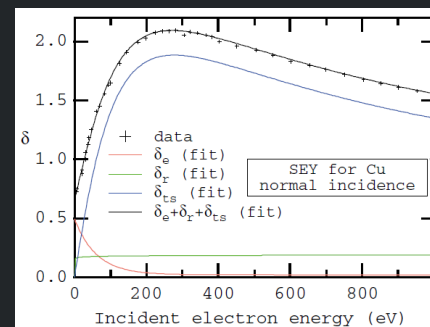
- Fitting to experimental data and the classification of secondary electrons



Choice of the energy distribution model determines the secondary electron classification:

$$\int_0^{E_0} f_{\{ts,r,e\}}(E) dE = \delta_{\{ts,r,e\}}(E_0),$$

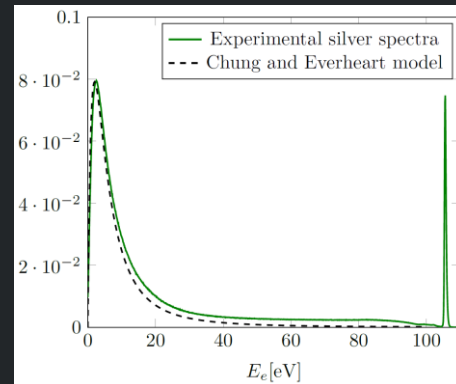
$$\delta_{ts} + \delta_r + \delta_e = \delta$$



D. Eremin, Secondary Electron Emission Models in PIC

- Chung-Everhard (physics-based) energy distribution

$$f(E) = 6W^2 \frac{E}{(E + W)^4}$$



[Villemant et al., 2017]

- Acceptance-rejection method [Nanbu and Oshita, 2013]

- 1) Make a trial $E = E_{\max} r_1$
- 2) Calculate $g(E) = f(E)/f_{\max}(E)$
- 3) If $r_2 < g(E)$, the trial value E is accepted

Using the acceptance-rejection method, it is possible to implement an arbitrary energy distribution

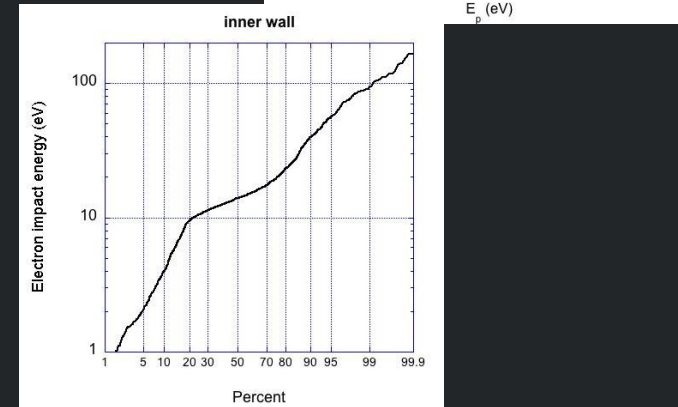
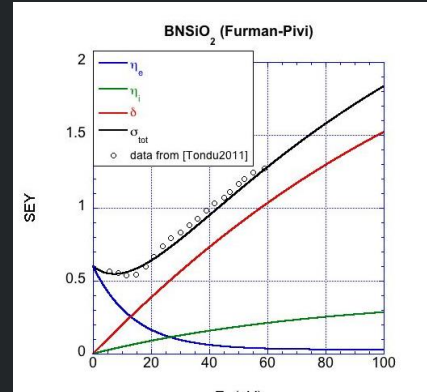
Taccogna, SEE

- Uncertainties on SEY in the low-energy range $E_p < 10$ eV
- The most accurate measurement [Tondu2011] and theoretical works [] suggest a saturation value or increasing SEY for decreasing energy $\Rightarrow \sigma(0) \neq 0$
- This is due to the contribution of (elastic and inelastic) backscattering to total SEY; backscattering is the dominant electron emission mechanism for $E_p < 20$ eV
- Common used fitting formula (linear, power law, Vaughan, etc.) are not appropriate
- Self-consistent radial (1D and 2D) PIC model (kinetic with non-Maxwellian EEDF) shows that:
 - electron-wall collision is a very important process
 - the majority (70%) of electrons impact the wall with $E_p < 20$ eV
- Suggested model (Furman-Pivi): $\sigma_{tot} = \eta_e + \eta_i + \delta$

Elastic backscattering: $\eta_e = \eta_{e\infty} + (\eta_{e0} - \eta_{e\infty}) e^{-\frac{E}{E_{e1}}} \quad \text{(blue curve)}$

Inelastic backscattering: $\eta_i = \eta_{i\infty} \left(1 - e^{-\frac{E}{E_{i1}}}\right) \quad \text{(green curve)}$

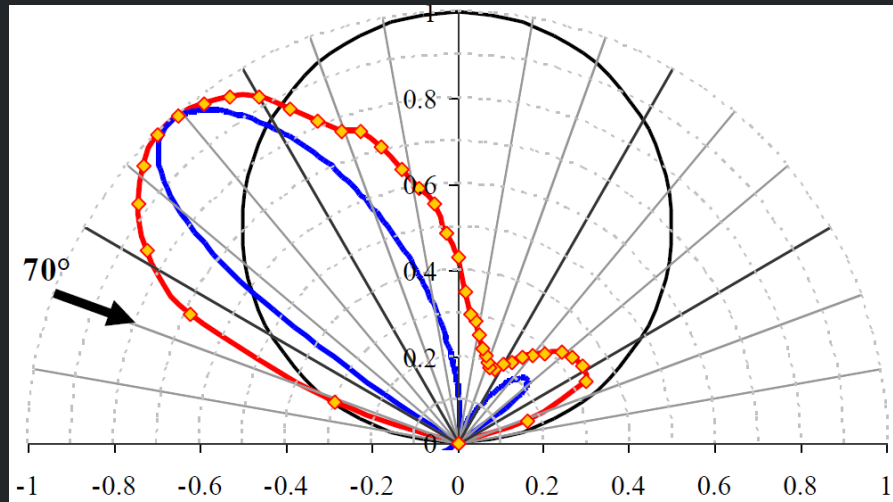
True secondary: $\delta = \delta_{max} \frac{t_1 \frac{E}{E_{max}}}{t_1 - 1 + \left(\frac{E}{E_{max}}\right)^{t_1}} \quad \text{(red curve)}$



Process	Frequency
Electron-neutral (Xe) collision	$\nu_{en} \approx 10^6 \text{ s}^{-1}$
Electron-ion (Xe+) collision	$\nu_{ei} \approx 10^5 \text{ s}^{-1}$
Anomalous collision	$\nu_{ano} \approx 10^7 \text{ s}^{-1}$
Electron-wall collision	$\nu_{ew} \approx 10^9 \text{ s}^{-1}$

Taccogna, SEE

- Backscattering electrons have memory effect on the emission energy and emission angle [Roupie13, Villemant19]:
- While true secondaries have an isotropic emission (cosine-Lambertian distribution, black curve on right →), backscattering electrons show a double-lobe emission (red curve on right →) corresponding to the incident and to the specular angle
- Important consequences:
 - stronger non-locality \Rightarrow electrons emitted from one wall are often those impacting on the opposite wall;
 - realistic estimation of the near-wall contribution on the electron anomalous mobility
- Sensitivity to $\sigma(0)$ in 1D(r) PIC model



	σ_{tot} IN / OUT wall	η_e IN / OUT wall	η_i IN / OUT wall	δ IN / OUT wall
Case 1: $\sigma(0)=0.4$	0.51 / 0.73	0.17 / 0.11	0.07 / 0.11	0.27 / 0.51
Case 2: $\sigma(0)=0.6$	0.58 / 0.74	0.28 / 0.16	0.10 / 0.11	0.28 / 0.47
Case 3: $\sigma(0)=0.8$	0.68 / 0.79	0.32 / 0.19	0.08 / 0.12	0.28 / 0.48

F. Cichocki et al.

Interaction of heavy species with walls

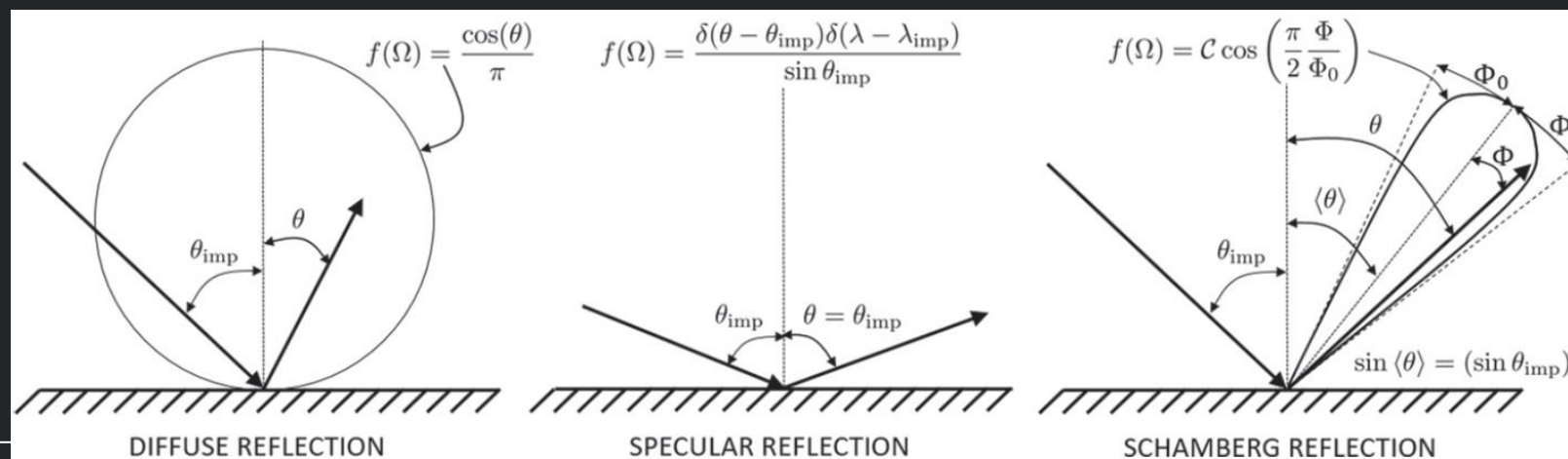
Importance of modeling heavy-particles wall interaction

- Plasma thrusters are devices with a **relatively high surface-to-volume ratio**
 - Surface interaction phenomena play a key role in determining their efficiencies
- Characterization of the ion/neutral wall interaction mainly requires modeling of:
 - **Angular distribution of reflected neutrals** → seen to affect the required mass flow for ignition [Dominguez et al, 2021]
 - **Emission energy of recombined neutrals** → strong influence on thruster performance [Ahedo et al, 2003]
- Re-emitted particle energy generally follows a law of the type:

$$\langle E \rangle = (1 - \alpha_W) \langle E_{\text{imp}} \rangle + \alpha_W E_W$$

energy accommodation coefficient average impacting particle energy
← wall energy ($E_W = 2T_W$)

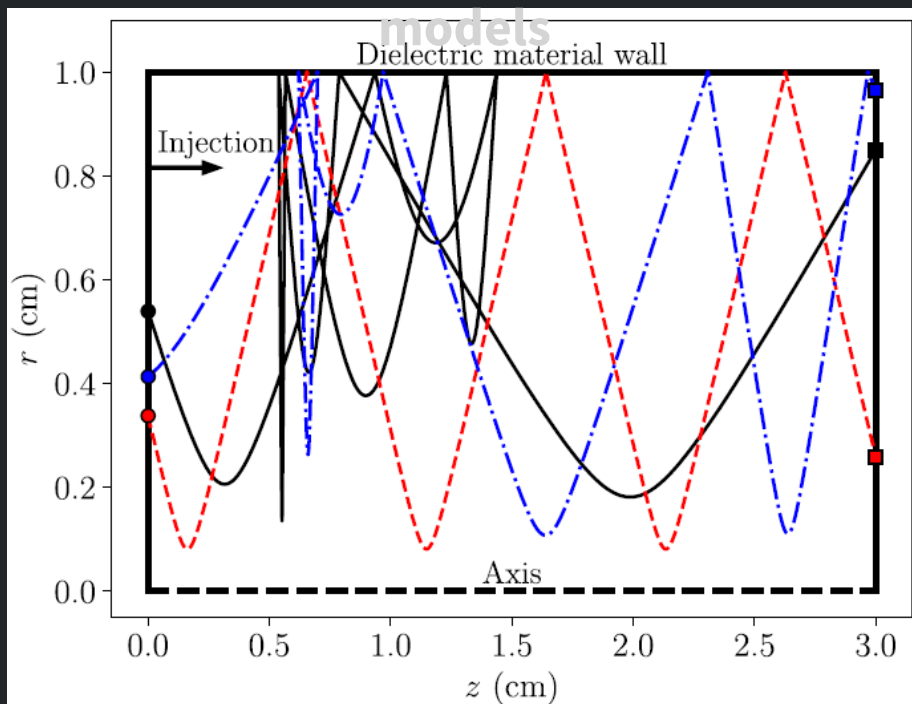
- Angular distribution of emitted particles can depend on impacting direction in complex ways. Three main types generally assumed: **DIFFUSE** (Lambert emission) **SPECULAR** or **SCHAMBERG** (both super-specular or sub-specular emission)



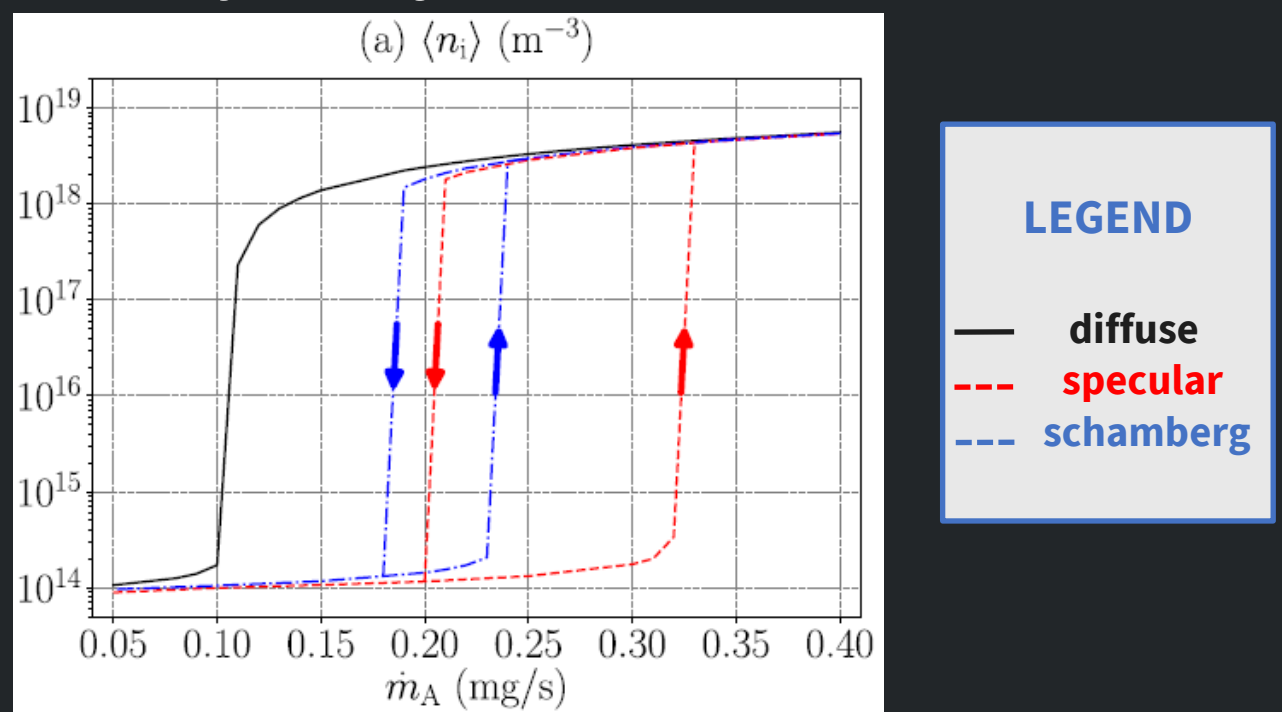
Effects of neutral reflection direction

- **EFFECTS IN AN CYLINDRICAL CHANNEL WITH INJECTION ON THE LEFT, AND OPEN BOUNDARY ON THE RIGHT** [Domínguez 2021]
 - Results obtained with a hybrid model (Maxwellian electrons and PIC ions/neutrals). No energy loss of reflected neutrals ($\alpha_W = 0$)
 - The diffuse reflection yields the highest residence times in chamber, yielding to the lowest required mass flow for a sustained discharge
 - A hysteresis cycle is observed on the average plasma density as injected mass flow is varied, only for non-diffuse reflections

Neutral trajectories for various refl.



Hysteresis cycle of average plasma density with injection mass flow



Effects of accommodation coefficient α_W for ion recombination

- **EFFECTS IN A CYLINDRICAL CHANNEL WITH INJECTION ON THE LEFT AND OPEN BOUNDARY ON THE RIGHT**

[Dominguez 2021]

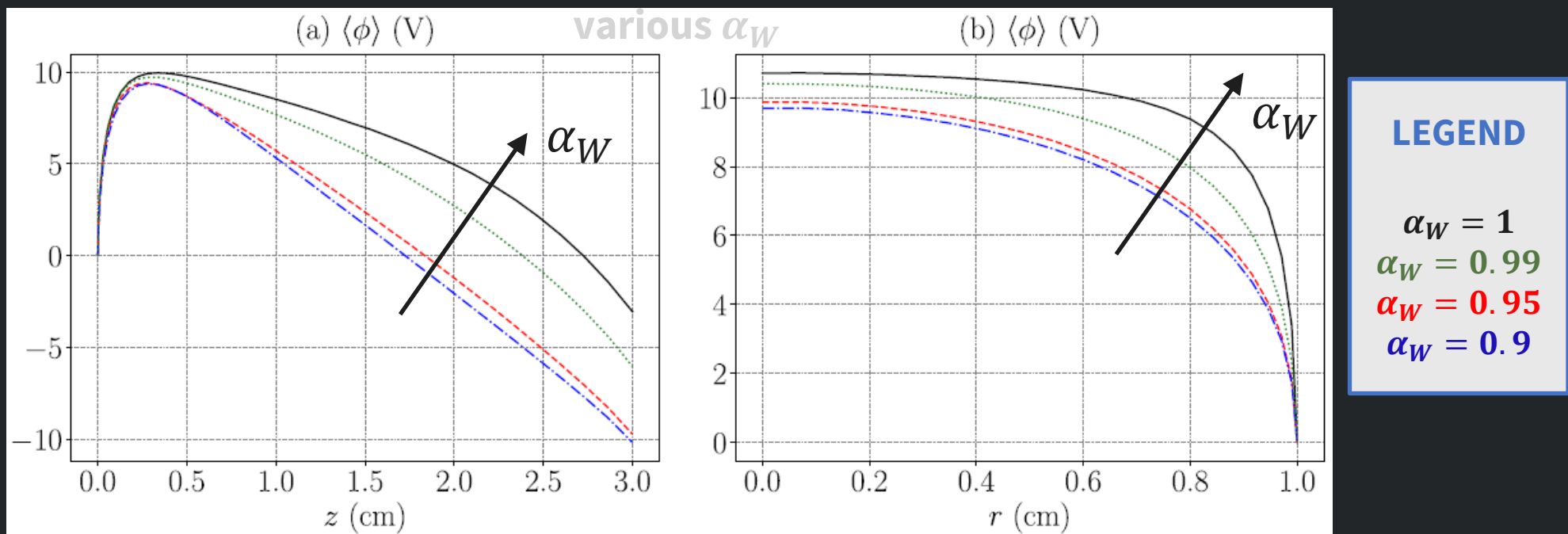
- Plasma profiles are extremely sensitive to small changes in the energy accommodation coeff. for ion recombination
- In this simplified scenario, the utilization efficiency lowers from 80% down to 20% for α_W changing from 1 to 0.9

- **EFFECTS IN A HALL THRUSTER DISCHARGE** [Ahedo 2003]

- Some studies (Ahedo 2003) report -10% of thrust efficiency for α_W decreasing from 1 to 0.9

Evolution of the electric potential along the axial (left) and radial (right) coordinate for

A DIFFUSE
EMISSION OF
RECOMBINE
D NEUTRALS
IS ASSUMED



Conclusions

- Both neutral reflection direction and accommodation coefficient for ion recombination play a relevant role in the discharge of electric thrusters
- Very few experimental studies exist to characterize the neutral scattering from solid surfaces
 - Most studies are relative to energy accommodation and angular distribution of reflected hypersonic neutrals (for atmosphere interaction in orbit)
 - Nearly no study is available for the low-energy scattering of Xe/Ar neutrals over dielectric walls
- Energy accommodation coefficients for ion recombination are also seldomly characterized experimentally and even less for ions/materials relevant for electric propulsion
 - Very precise estimation of α_W are required to enable precise thruster predictions
- Experimental campaign needed to produce a database **on low energy neutral scattering and ion recombination coefficients** for the electric propulsion community. Is it possible?

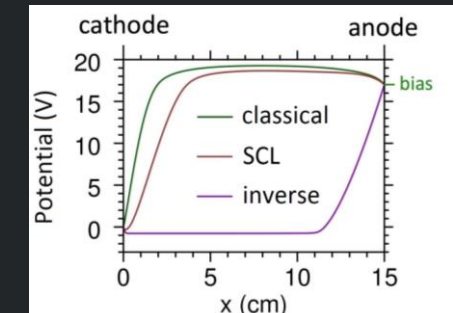
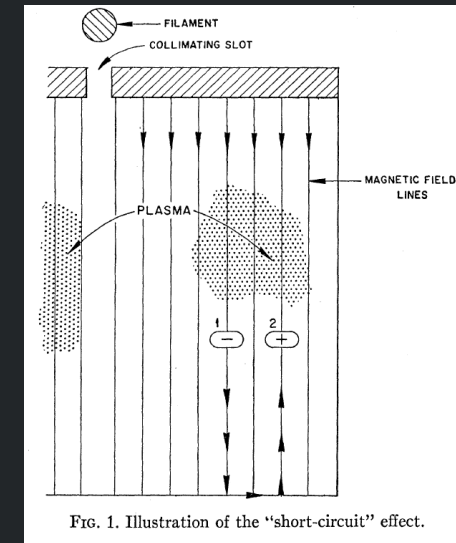
Y. Raitses

Active Boundaries

for $E \times B$ Plasmas

Y. Raitses, Active Boundaries for $E \times B$ Plasmas

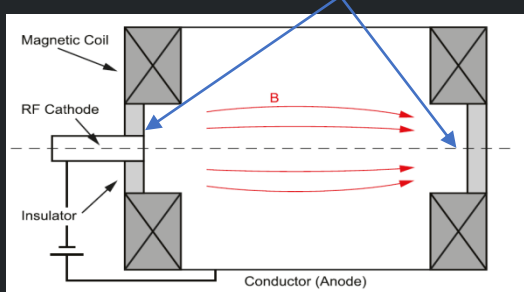
- **Objective: Control of the $E \times B$ plasma with biased walls/electrodes**
 - Effect on spatial distribution of plasma properties (for HT, placement of the acceleration)
 - Suppression of low frequency oscillations
 - Effect on cross-field transport
 - Effect on performance, plasma plume
- Previous relevant research on **fully magnetized plasmas** and **partially magnetized plasmas**
 - Short circuit effect on plasma in B-field (A. Simon, Phys. Rev. 98, 317 (1955))
 - Biased electrodes to control $E \times B$ transport, plasma stability and confinement in magnetic fusion devices (e.g., biased electrodes for magnetic mirrors and FRCs, tokamak divertors (NSTX), centrifugal confinement (MCX), LAPD (UCLA))
 - Plasma mass separation in $E \times B$ (Archimedes Technol.)
 - Control of transport and plume in plasma thrusters (segmented electrode Hall thruster – experiments at PPPL, Aerospace Corp., CNRS, modeling at the GWU, PPPL, U Sask.)



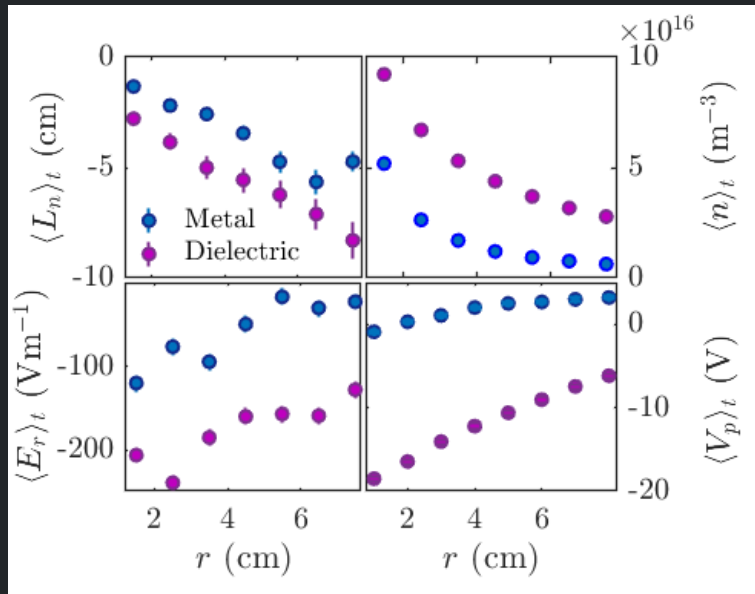
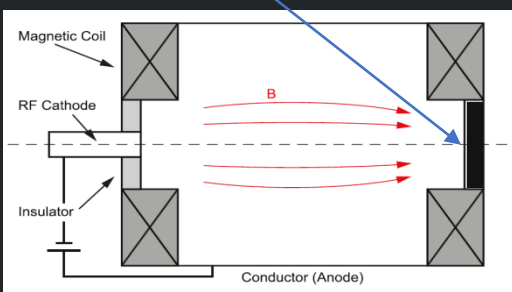
M. Campanell, 2017

Y. Raitses, Biased Wall for $E \times B$ Penning Plasmas¹

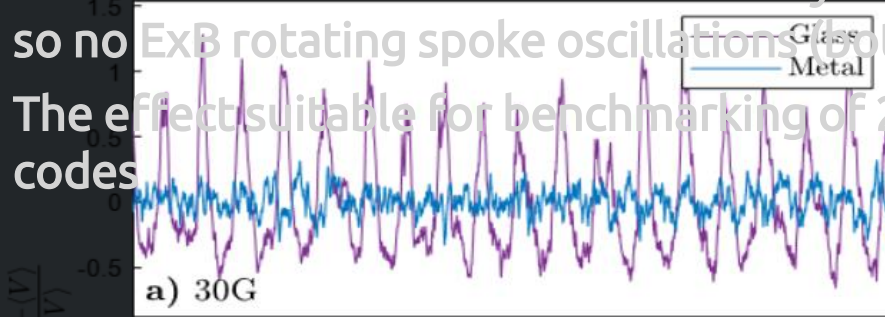
Dielectric (glass) side walls



Anode-based metal walls

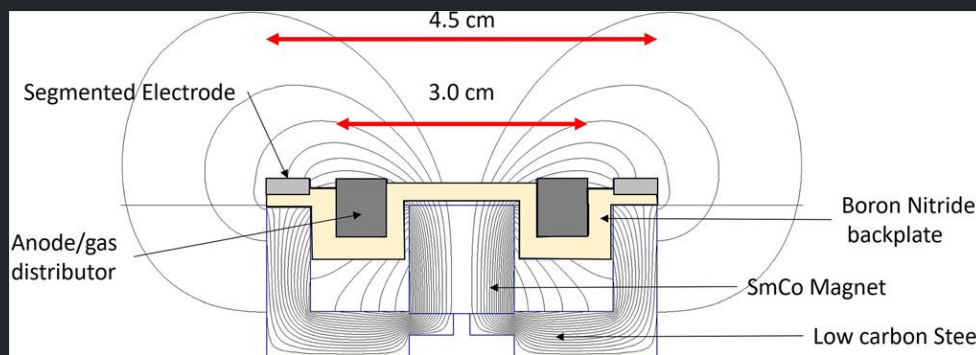


- Linear device with partially magnetized plasma in applied $E \times B$ fields
- Plasma is generated by the electron beam/energetic electrons extracted from the RF cathode (left top Figs.)
- Two cases: 1) dielectric boundaries with plasma electrons confined by plasma-wall sheath and 2) anode - biased metal wall collecting electrons along B-field
- In the 2nd case, no significant E- field due to the smaller anode sheath and short circuit by the metal wall (left Fig.)
- No condition for Simon-Hoh instability $E \cdot \nabla n_0 > 0$ and so no $E \times B$ rotating spoke oscillations (bottom Fig.)
- The effect suitable for benchmarking of 2-D and 3-D codes

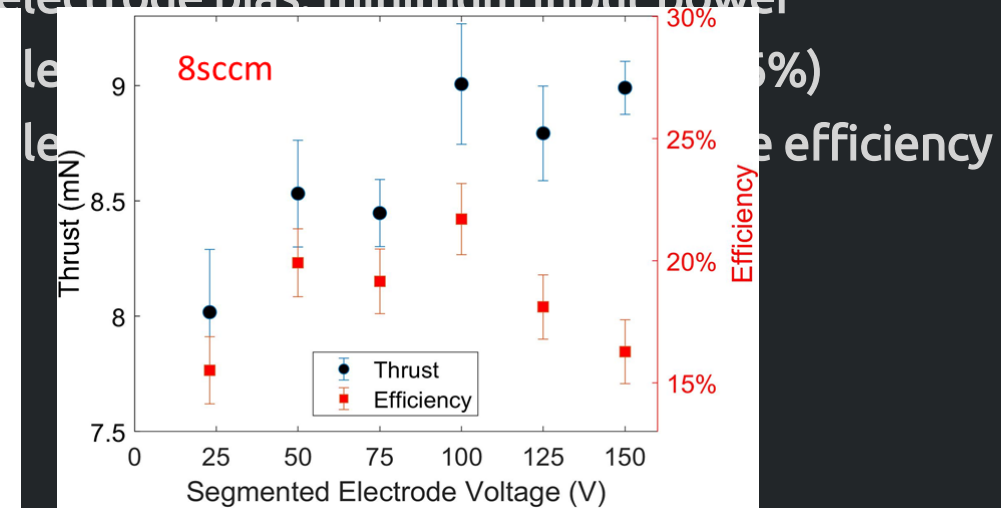
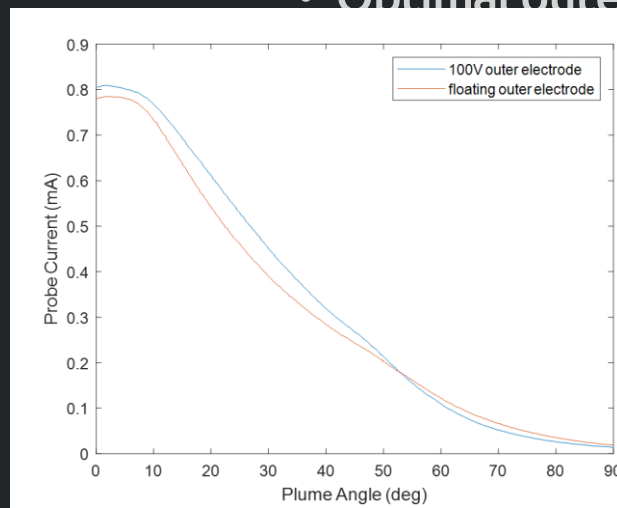
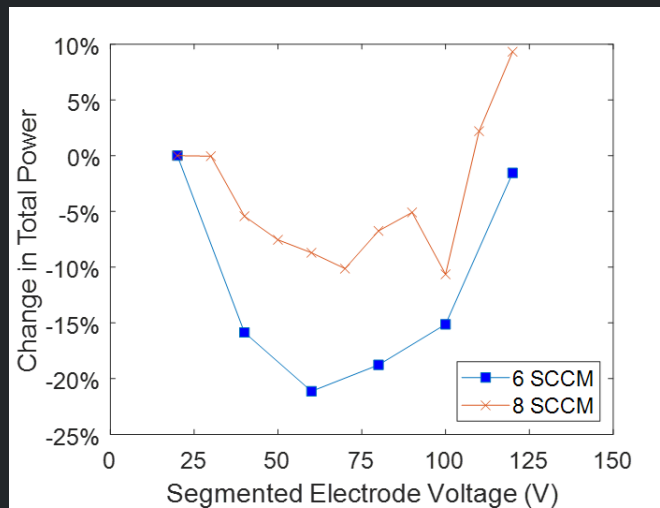


¹ E. Rodriguez et al., "Boundary-induced effect on the spoke-like activity in $E \times B$ plasma", Phys. Plasmas 26, 053503 (2019)

Y. Raitses, Segmented Electrodes for Hall Thrusters²

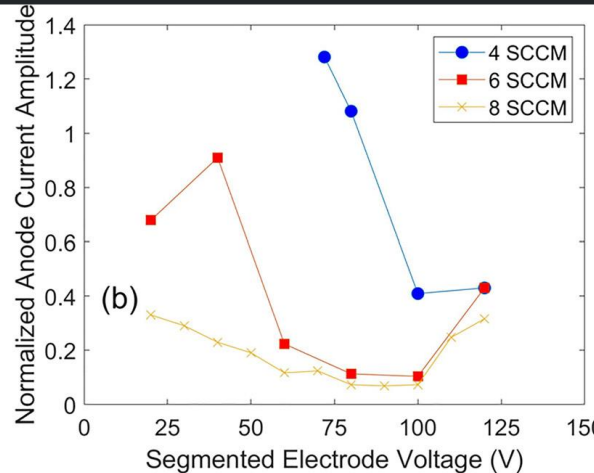
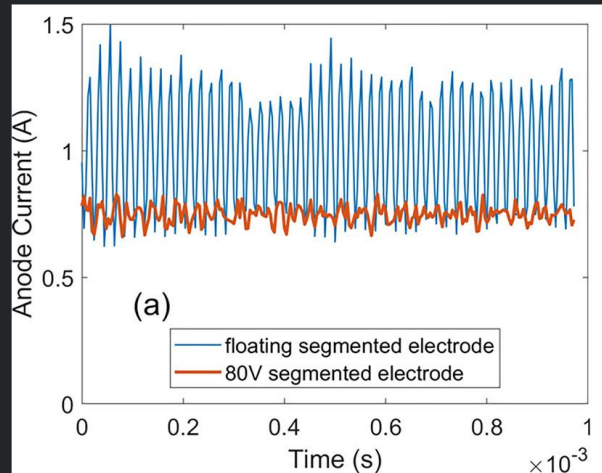
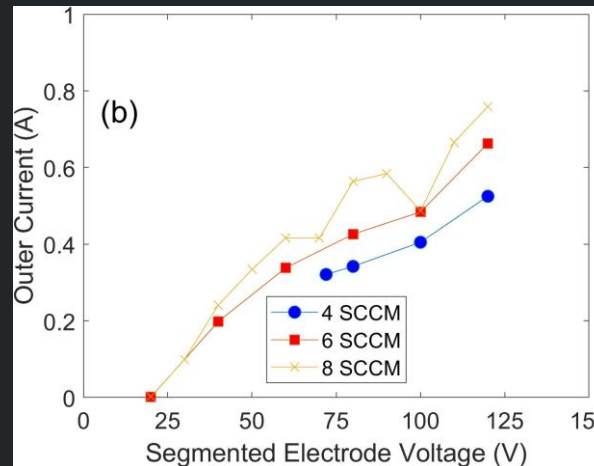
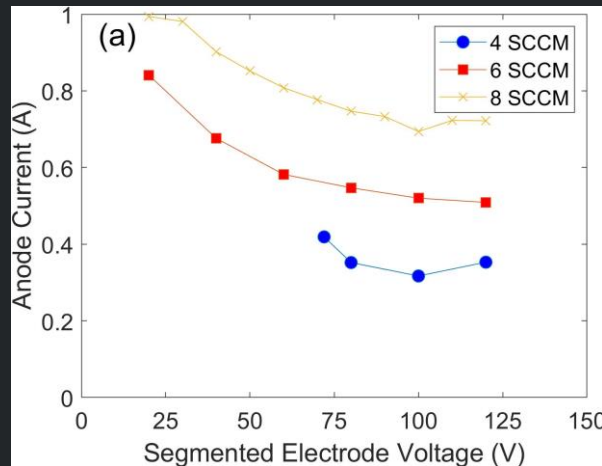


- 100-200 W Wall-less Hall thruster with outer segmented electrode
- Parameters: $B \sim 1$ kGauss, $V_d \sim 200-400$ V, Xe flow 4-8 SCCM
- Anode- gas distributor, but no flow through the outer electrode
- Biasing outer electrode 0- + 125 V with respect to the cathode
- Optimal outer electrode bias: minimum input power



² J. Simmonds and Y. Raitses, "Mitigation of breathing oscillations and focusing of the plume in a segmented electrode wall-less Hall thruster", *Appl. Phys. Lett.* **119**, 213501 (2021)

Y. Raitses, Segmented Electrodes for Hall Thrusters²



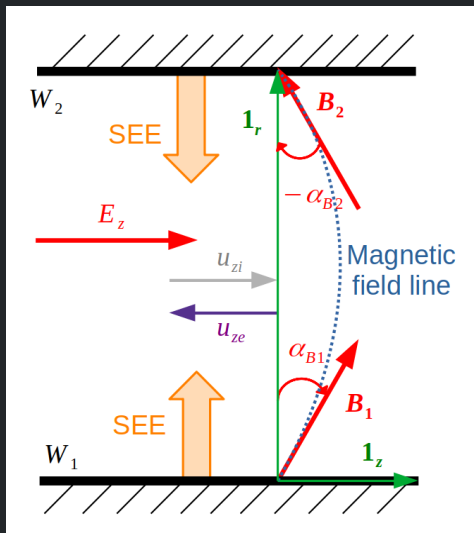
- As outer electrode bias increases
 - Outer electrode current increases
 - Anode current decreases
 - Breathing oscillations are the same frequency for both electrodes, but phase shifted $\sim 50^\circ$
- Breathing mode is suppressed in both electrodes when the outer current is comparable to the anode current.
- Physical mechanism of the suppression is not understood, but possibly connected to the phase shift between parallel discharges.

² J. Simmonds and Y. Raitses, "Mitigation of breathing oscillations and focusing of the plume in a segmented electrode wall-less Hall thruster", *Appl. Phys. Lett.* **119**, 213501 (2021)

A. Marín et al.

Kinetic modeling of electron wall interaction

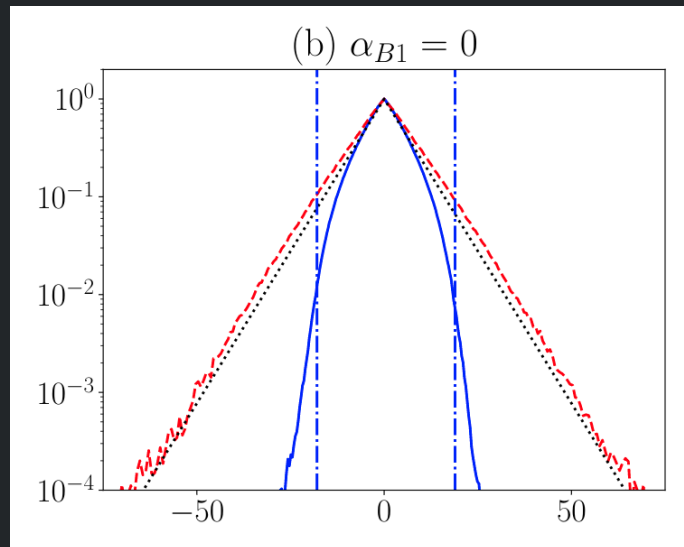
A. Marín et al., 1Dr kinetic simulations in HETs



- Case: B purely radial
- Kinetic VDF shows **strong radial depletion**
- Wall interaction parameters of interest:
 - Electron current density: j_{reW}
 - Energy collected electron: \mathcal{E}_{eW}
- Values for Maxwellian VDF:

$$j_{reW}^{*} = en_{eQ} \exp \left(-\frac{e\phi_{WQ}}{T_{eQ}} \right) \sqrt{\frac{T_{eQ}}{2\pi m_e}},$$

$$\mathcal{E}_{eW}^{*} = 2T_{eQ} + m_e u_{eW}^2 / 2$$



- Ratios for depleted vs Maxwellian VDF:

$$\sigma_{rp} = |j_{reW}^{(tw)}| / j_{reW}^{*} \ll 1$$

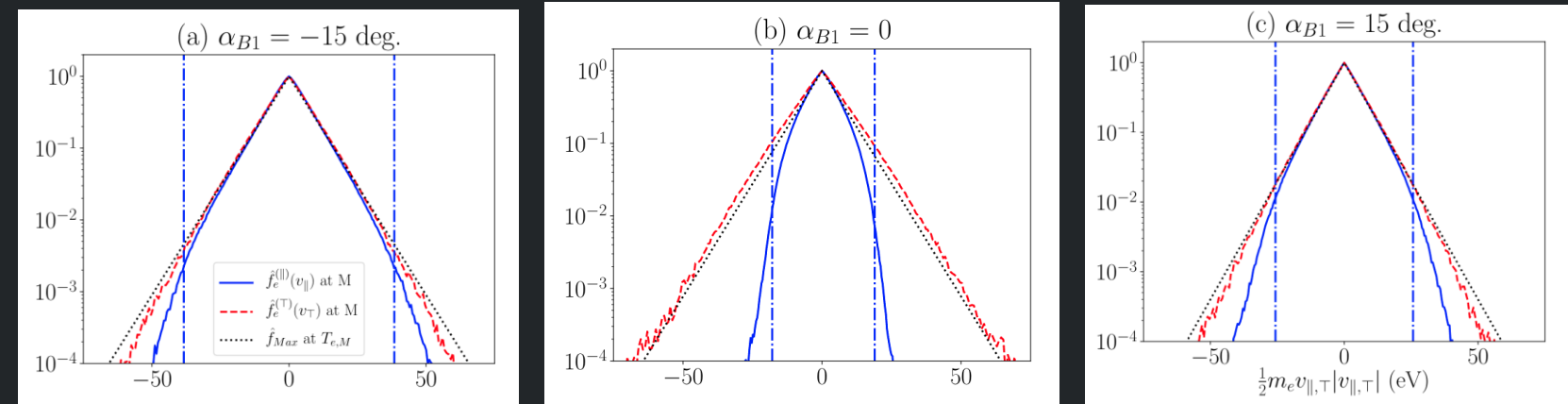
$$\Theta = \mathcal{E}_{eW} / \mathcal{E}_{eW}^{*}; \quad \sim 1$$

Table 3. Electron-wall interaction magnitudes for cylindrical and planar configurations.

Type and units	Symbol	N	I	A
ANNULAR CHANNEL				
Current densities to walls (A m^{-2})	$ j_{reW1}^{(tw)} $	82	345	133
	$ j_{reW2}^{(tw)} $	127	665	950
Average electron impact energy (eV)				
	\mathcal{E}_{eW1}	8.3	30.1	14.9
	\mathcal{E}_{eW2}	16.5	50.1	65.0
SEE yields (-)				
	$\langle \delta_{s,1} \rangle$	0.16	0.46	0.26
	$\langle \delta_{s,2} \rangle$	0.30	0.72	0.83
Electron current density ratio (-)				
	σ_{rp1}	0.05	0.13	0.05
	σ_{rp2}	0.06	0.18	0.04
Electron energy ratio (-)				
	Θ_1	0.62	0.52	0.40
	Θ_2	1.01	0.78	0.82
PLANAR CHANNEL				
SEE yields (-)	$\langle \delta_s \rangle$	0.22	0.63	0.79
Electron current density ratio (-)	σ_{rp}	0.03	0.12	0.01
Electron energy ratio (-)	Θ	0.77	0.67	0.70

A. Marín et al., 1Dr kinetic simulations in HETs

- **B oblique, $\alpha_{B2} = -\alpha_{B1}$**
- VDF is much less depleted
 - σ_{rp} much higher
 - $\Theta \sim 1$
- Oblique B facilitates radial-axial transfer in the electron VDF
- Cylindrical effects remain but asymmetries lower than in purely radial case

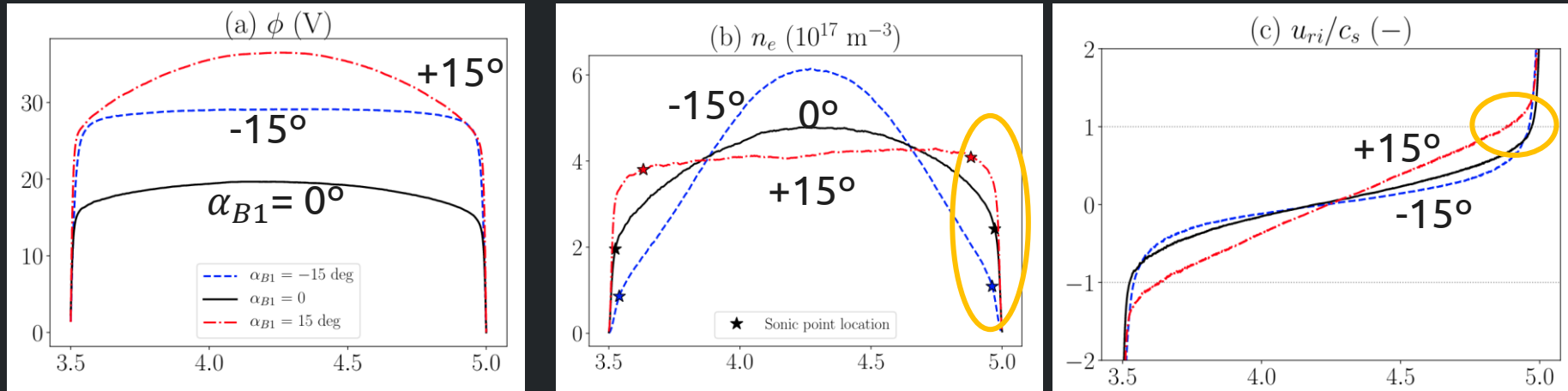


Magetic field angle (deg.)	α_{B1}	-15	-10	-5	0	5	10	15
Current densities to walls (A/m²)	$j_{re,1}^{(tw)}$	41	50	60	81	123	163	196
	$j_{re,2}^{(tw)}$	54	68	92	131	157	185	220
Average electron impact energy (eV)	$\langle \mathcal{E}_{e,1} \rangle$	10.64	9.33	8.99	8.53	9.26	10.35	10.76
	$\langle \mathcal{E}_{e,2} \rangle$	13.09	12.06	13.06	16.38	14.30	13.44	13.00
Macroscopic SEE yield (-)	$\langle \delta_{s,1} \rangle$	0.21	0.18	0.18	0.16	0.19	0.21	0.21
	$\langle \delta_{s,2} \rangle$	0.25	0.24	0.26	0.32	0.28	0.26	0.26
Replenishment factor (-)	$\sigma_{rp,1}$	0.28	0.21	0.11	0.06	0.15	0.34	0.49
	$\sigma_{rp,2}$	0.33	0.27	0.12	0.07	0.17	0.36	0.50
Energy ratio (-)	Θ_1	0.74	0.66	0.66	0.66	0.69	0.76	0.79
	Θ_2	0.82	0.77	0.81	1.01	0.92	0.88	0.85

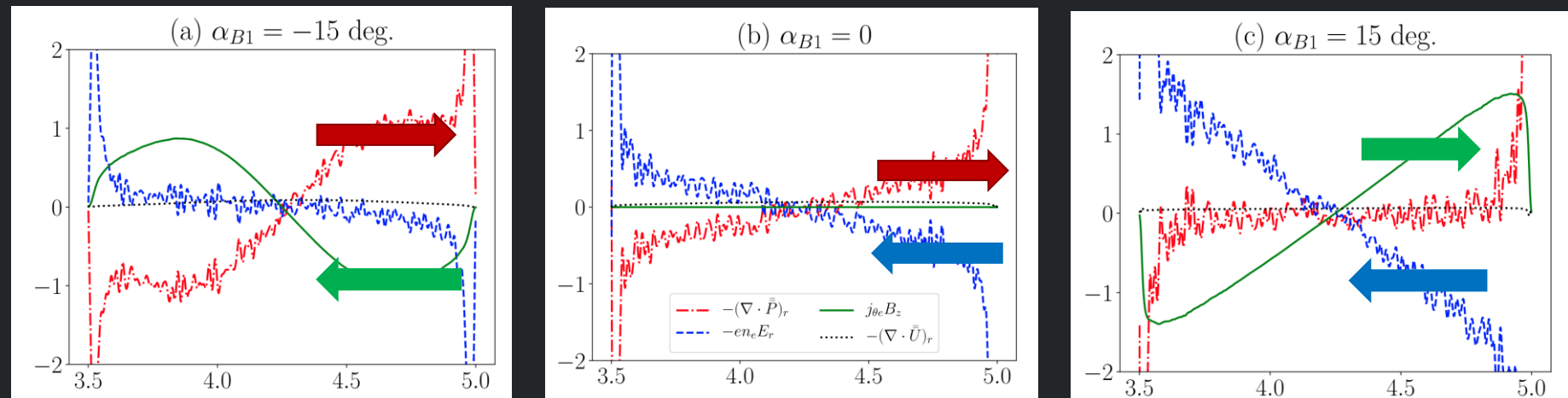
A. Marín et al., 1Dr kinetic simulations in HETs

B oblique, $\alpha_{B2} = -\alpha_{B1}$

- Macroscopic behavior:
 - Different behavior in radial balances between $\alpha_{B1} < 0$ and $\alpha_{B1} > 0$
- Radial magnetic force (due to) changes sign with α_{B1}
- Dominant terms in radial momentum change with α_{B1}
- Fluxes to wall higher for $\alpha_{B1} > 0$



$$0 \simeq j_{\theta e} B_z - (\nabla \cdot \bar{\bar{P}}_e)_r - e n_e E_r$$

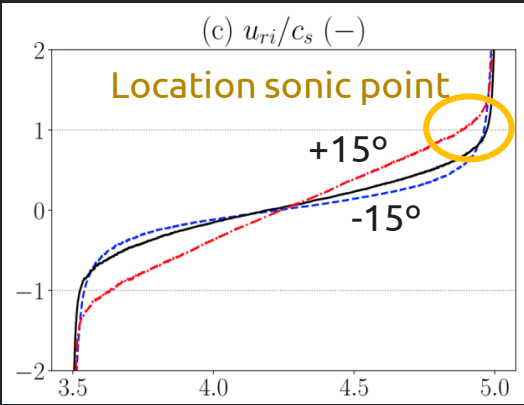


A. Marín et al., 1Dr kinetic simulations in HETs

B oblique, $\alpha_{B2} = -\alpha_{B1}$

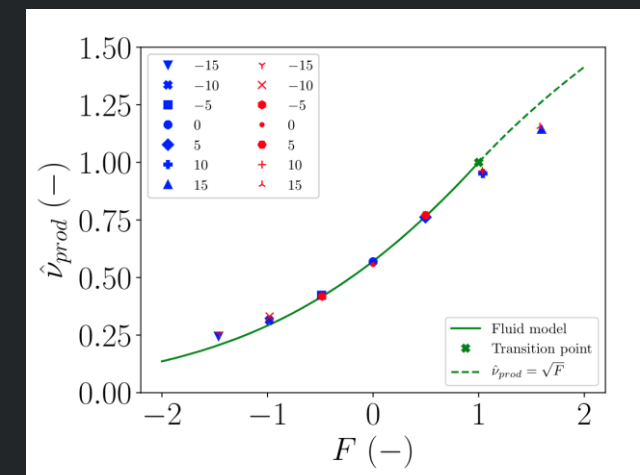
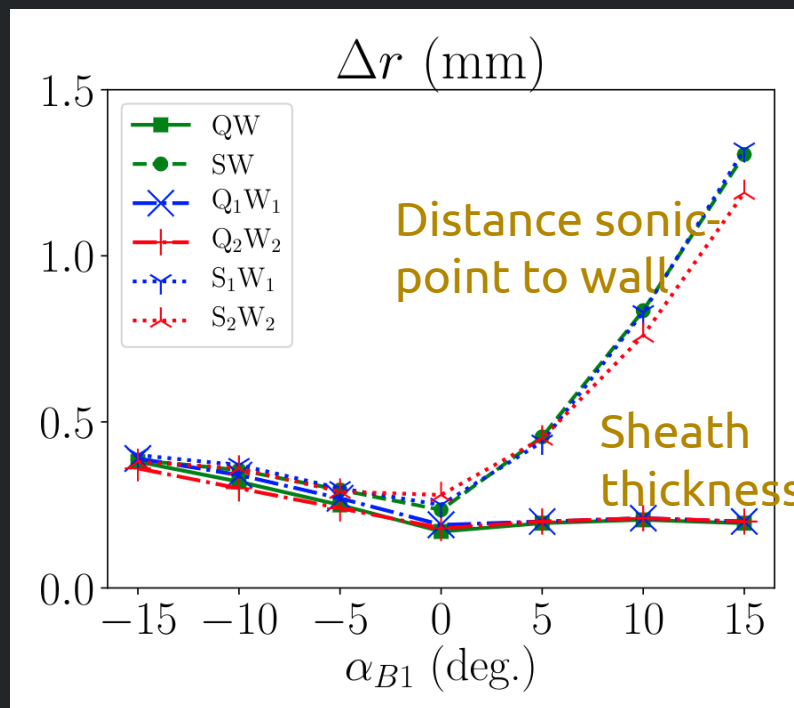
Unexpected result for α_{B1} positive and not small:

- Subsonic/supersonic (regular) transition within quasineutral plasma
- This means that plasma/sheath transition is supersonic
- A simple analytical fluid model corroborates this result
 - Excellent agreement with kinetic results



$$\begin{aligned} \frac{d}{dr}(n_e u_{ri}) &= n_e \bar{v}_{prod}, \\ m_i \frac{d}{dr}(n_e u_{ri}^2) &= -en_e \frac{d\phi}{dr}, \\ 0 &= -T_e \frac{dn_e}{dr} + en_e \frac{d\phi}{dr} - en_e E_z \tan(\alpha_B), \end{aligned}$$

Simple fluid model

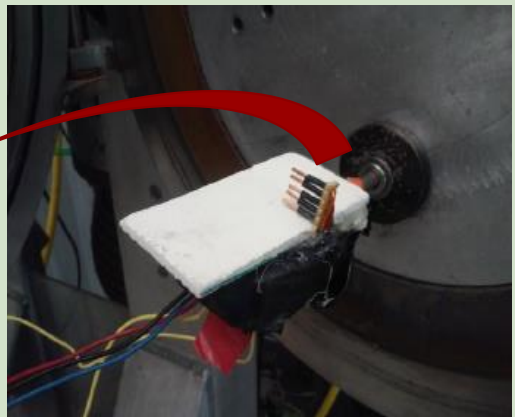
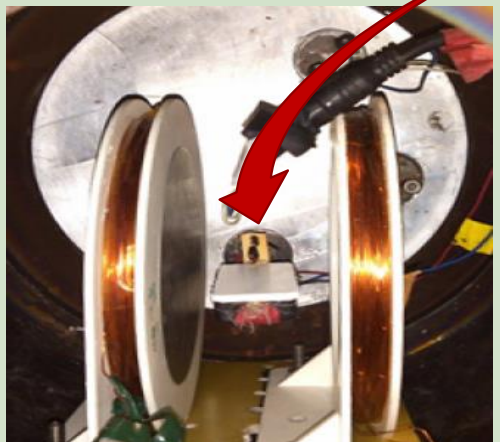
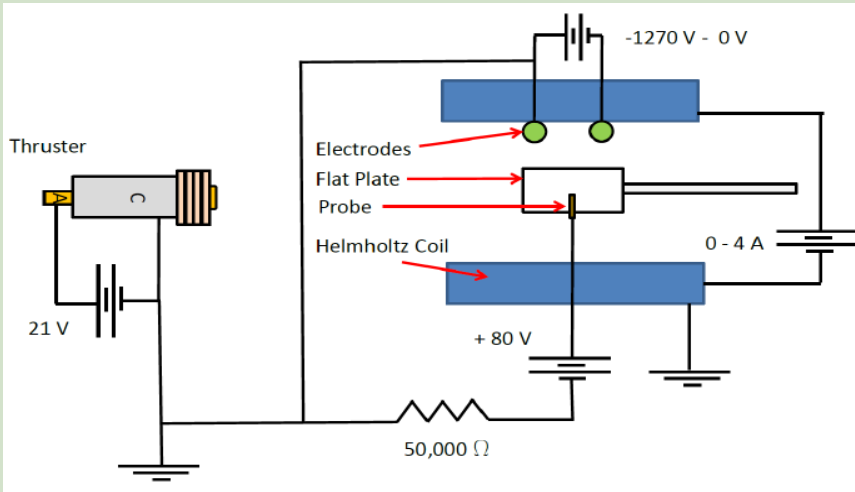


Agreement fluid and kinetic results

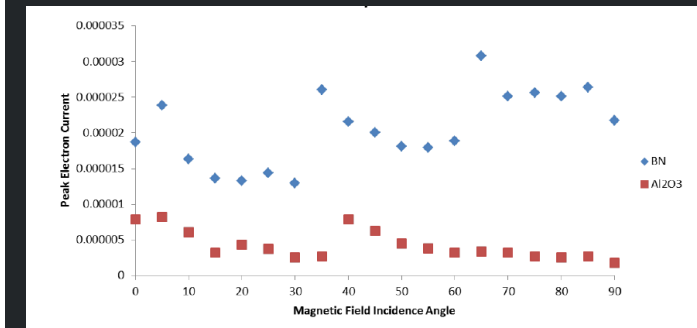
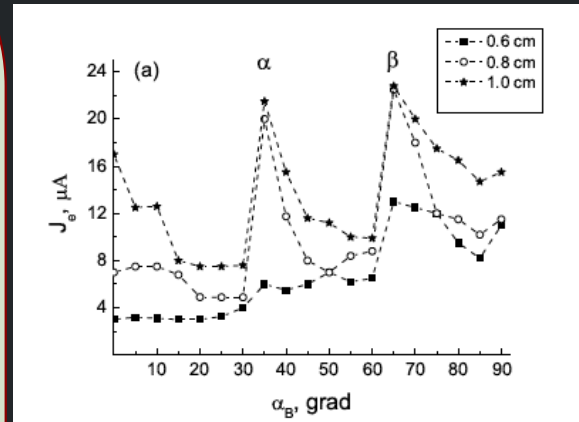
M. Keidar

Periodic structures in a magnetic field

Experiment observations

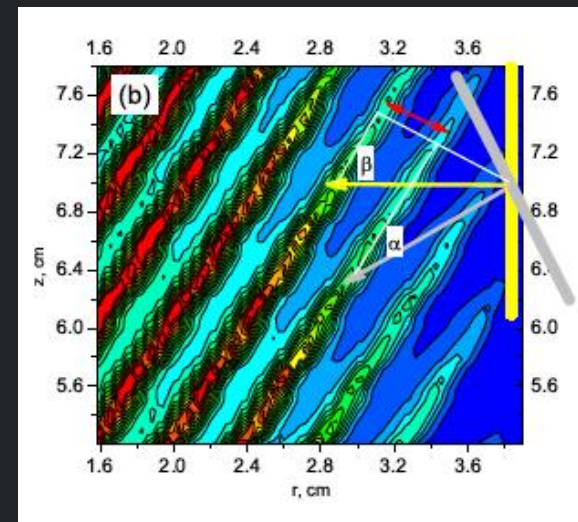


Periodic structure



Lukas JN, 2016, PhD Thesis, George Washington University

Simulations



Kinetic simulations

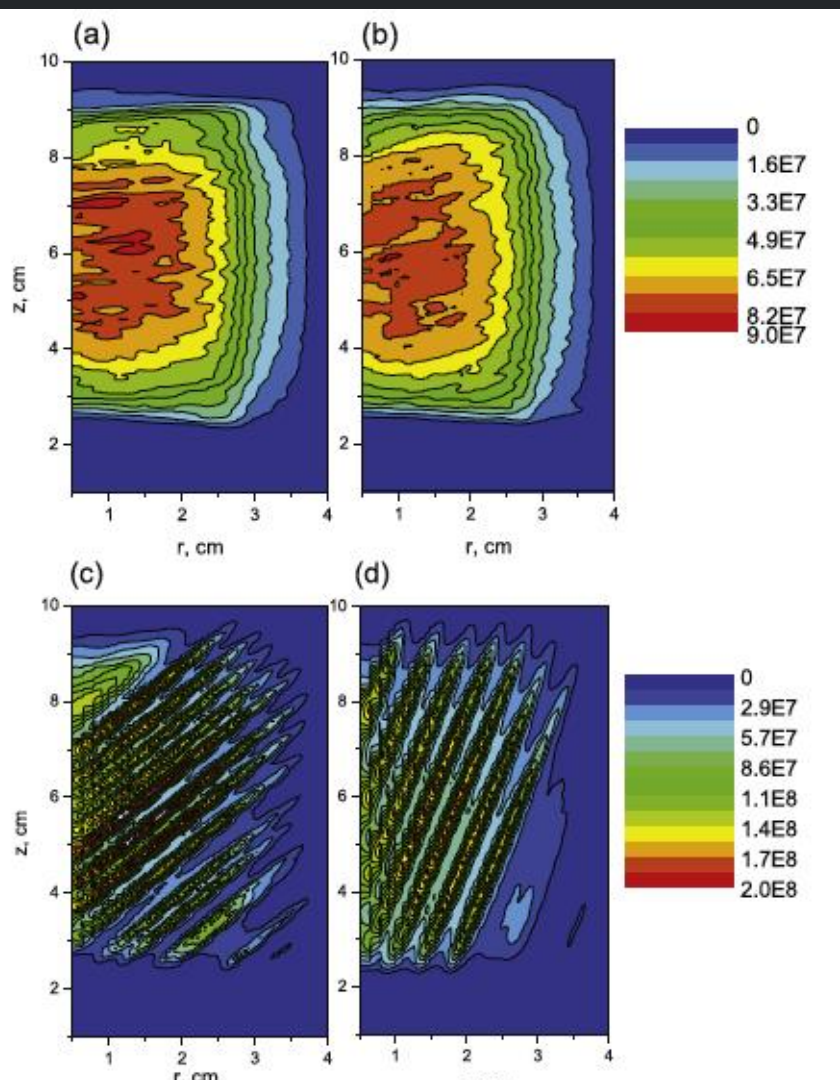
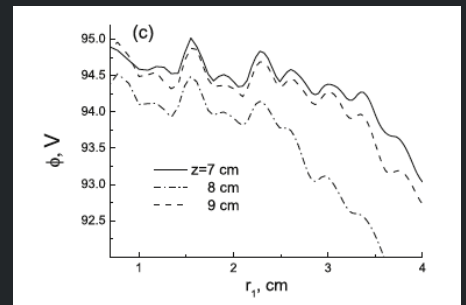
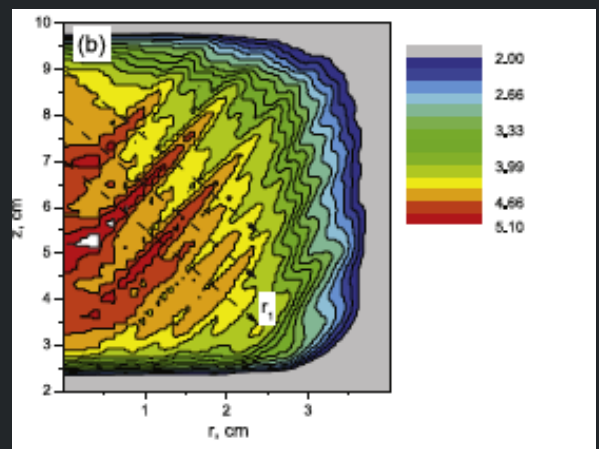
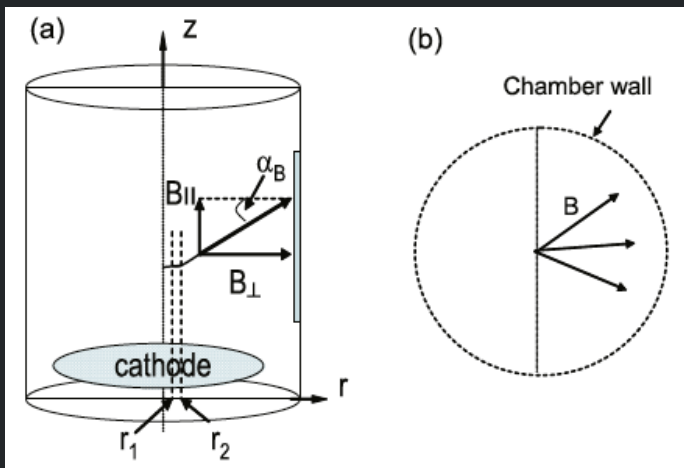
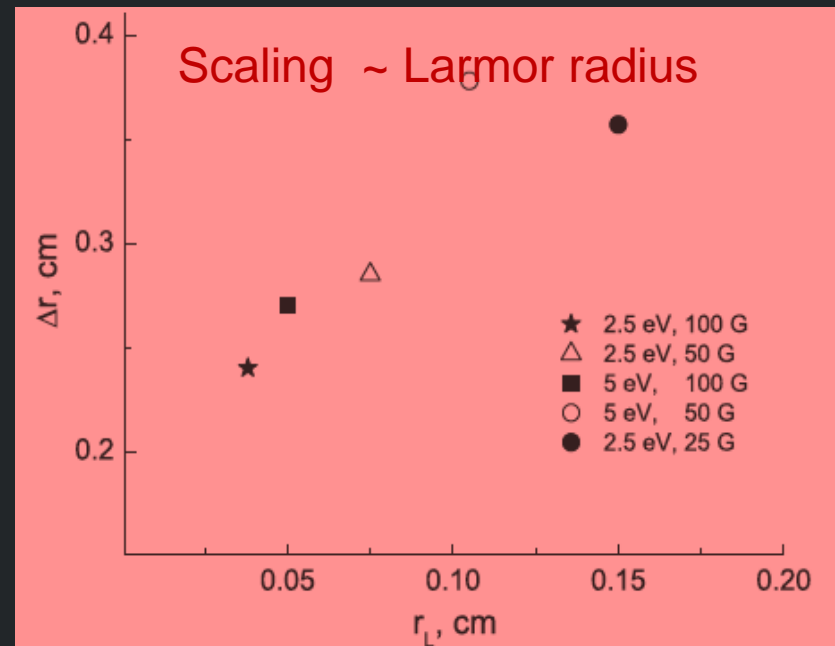


Figure 2. Distribution of electron density, n_e , cm^{-3} (linear scale), for $\alpha_B = 10^\circ$ (a), 27° (b), 55° (c) and 77° (d), $B = 50$ G, $T_e = 2.5$ eV.



J. Polk

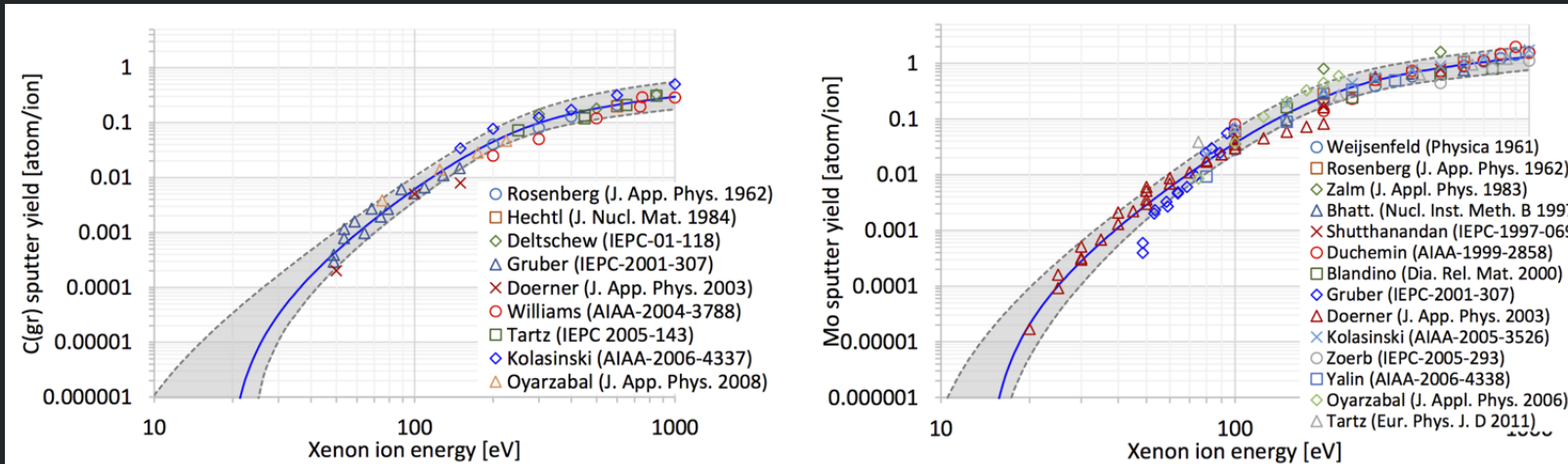
Pole Erosion Characterization Using Surface Layer Activation

Objective: A Rapid Survey to Determine What Drives Pole Erosion

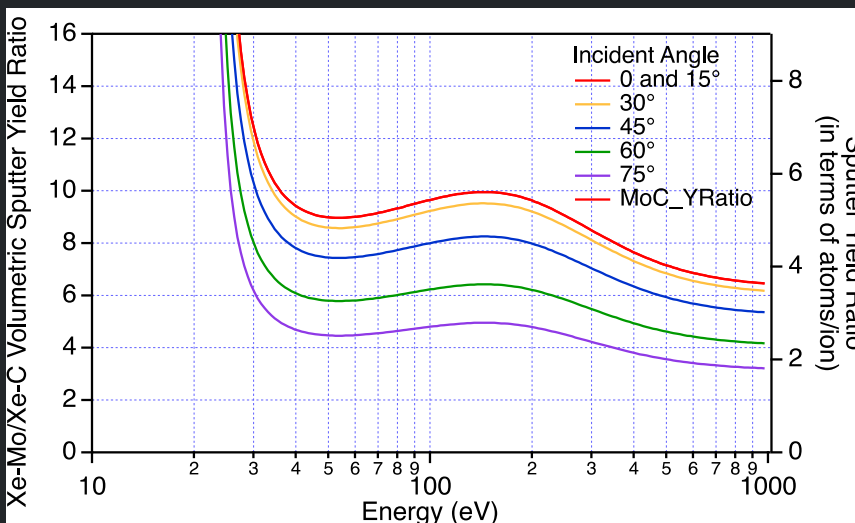
- **Characterize the pole erosion rates over a broad range of operating conditions**
 - Use Mo pole covers to accelerate wear rates
 - Use high sensitivity Surface Layer Activation (SLA) technique to get data in relatively short duration tests (8-12 hours)
- **Characterize erosion rates for nominal HERMeS operating conditions and identify the worst case**
- **Help define the operating condition(s) for future wear tests**
 - Resulted in a series of short duration wear tests with TDU-1 and TDU-3 (Williams, IEPC-2017-207, presented this morning)
 - Part of ongoing planning for upcoming EDU wear test
- **Determine sensitivity to discharge voltage and current (provide clues to mechanisms)**
- **Determine the effect of other parameters**
 - Magnetic field strength
 - Magnitude of discharge voltage ripple
 - Facility pressure effects

J. Polk, Pole Erosion Characterization Using Surface Layer Activation

Accelerated Wear Testing Using a Molybdenum Pole Cover



Yim, J, "A survey of xenon ion sputter yield data and fits relevant to electric propulsion spacecraft integration" IEPC-2017-060

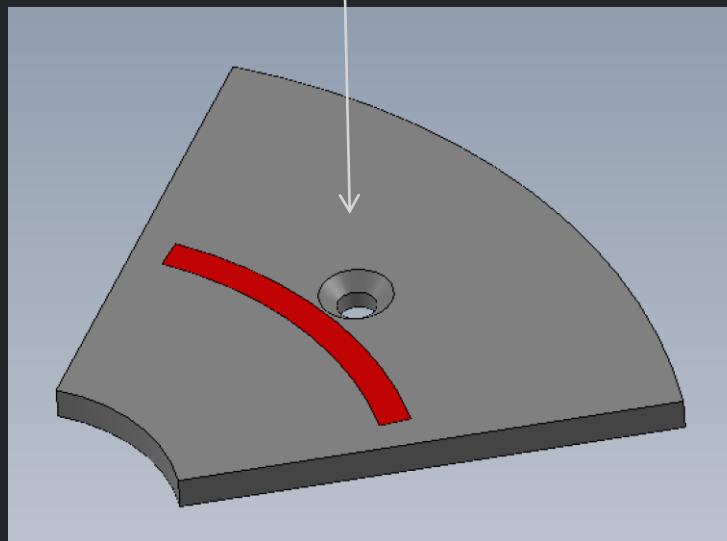


- Acceleration factor for normal incidence is 8 -10x
- Uncertainties in yield data make scaling rates to graphite difficult
- Primary value is in:
 - Defining relative erosion rates
 - Identifying primary drivers
 - Providing data to validate erosion models

J. Polk, Pole Erosion Characterization Using Surface Layer Activation

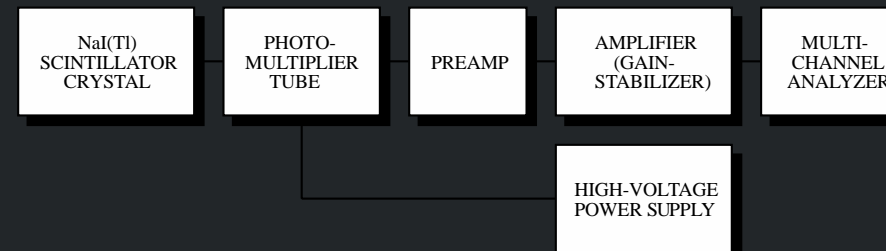
Surface Layer Activation Technique for Sub-Micron Erosion Measurement

1. Bombard Mo pole cover segments with 11 MeV proton beam to produce a thin layer (~100 nm) containing a small amount of gamma emitting ^{95m}Tc

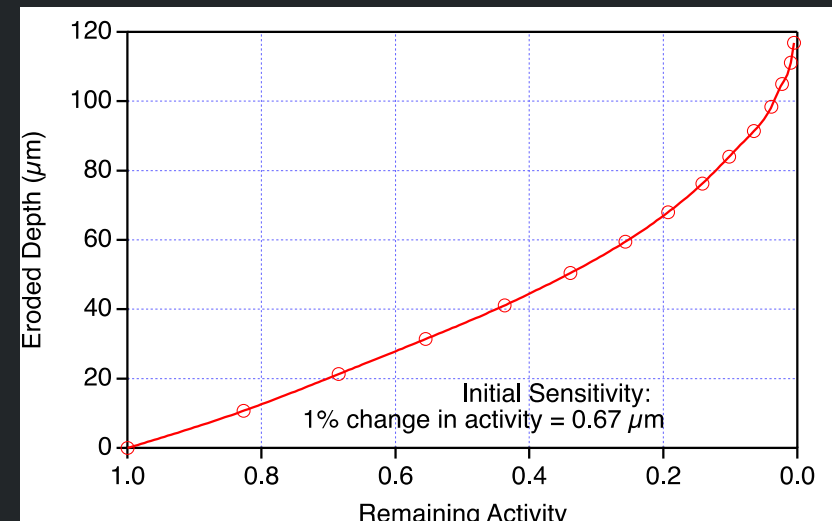


With sufficiently high signal strengths, SLA can be a real-time, in situ, non-intrusive direct measurement of erosion

2. Monitor activity level during operation with standard gamma ray spectrometry system

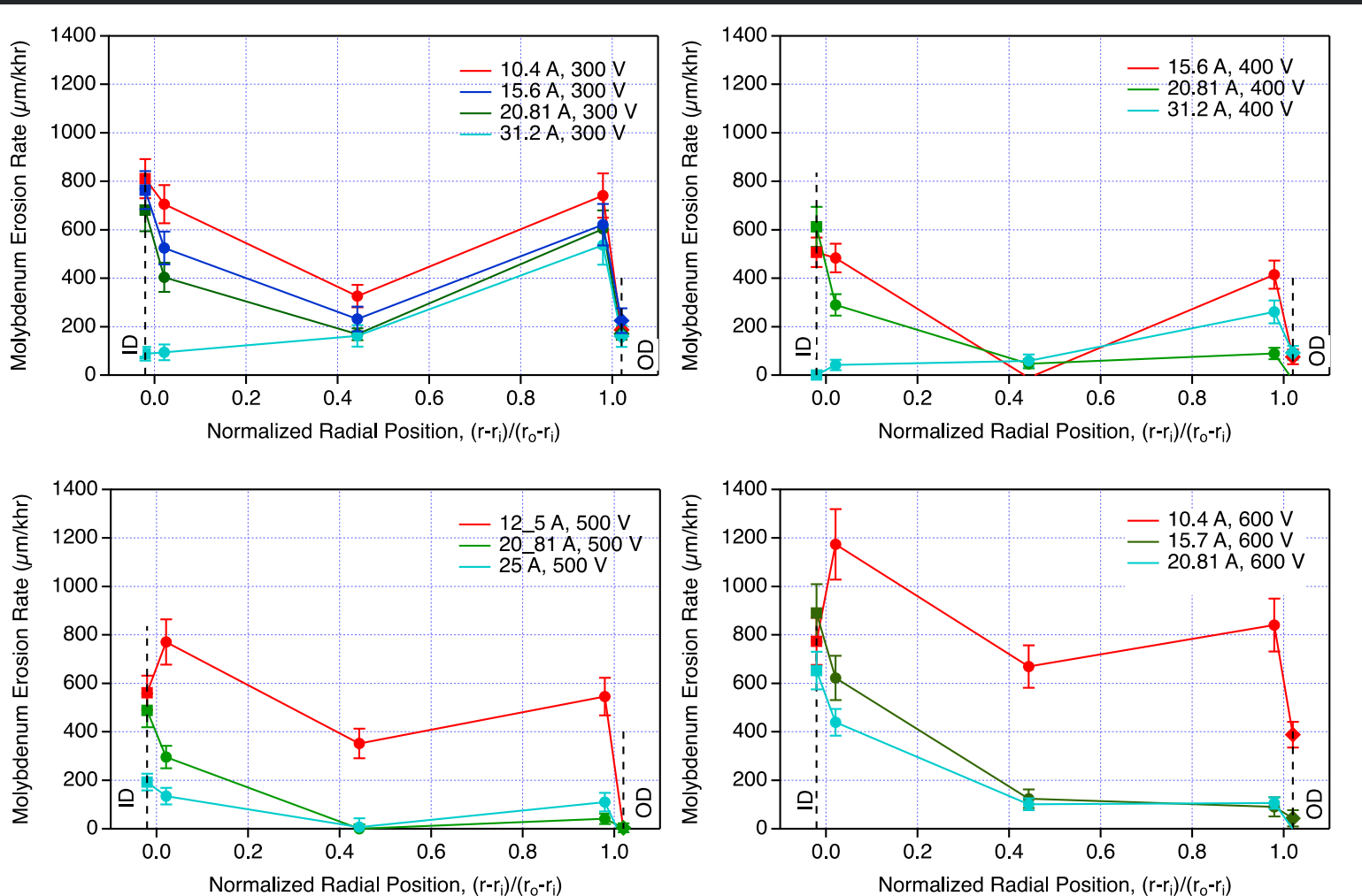


3. Calculate erosion depth based on fraction of remaining radioactivity using calibration curve



J. Polk, Pole Erosion Characterization Using Surface Layer Activation

Scaling with Discharge Current and Voltage



- **300 V is the worst case for the nominal HERMeS operating conditions (20.8 A, 300 – 600 V)**
- **Lowest currents are worst case; 31 A looks relatively benign**
- **Some other parameters also affect erosion**
 - Magnetic field strength: increasing erosion on ID and inner face with increasing **B**
- Magnitude of discharge voltage ripple: no effect
- Facility pressure effects: Increasing pressure suppresses inner face and ID erosion; short duration wear test data are unclear



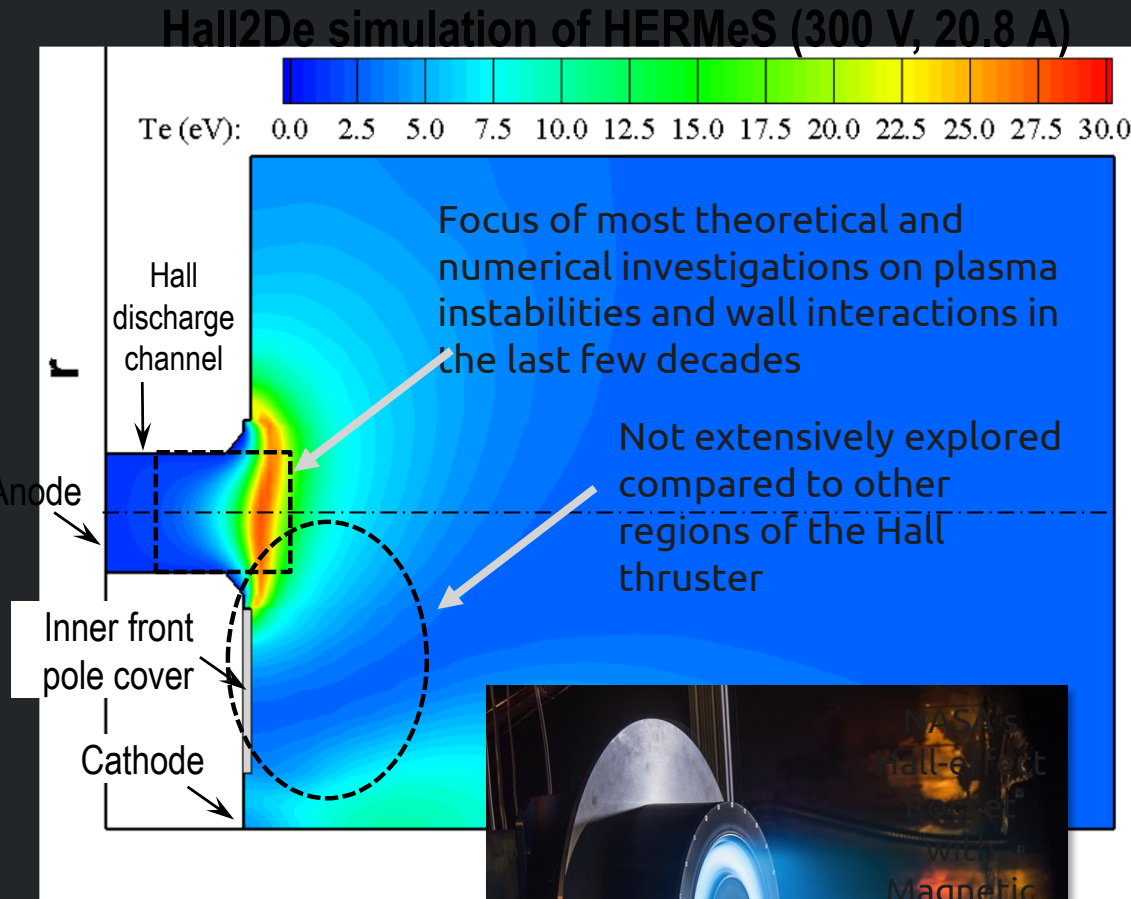
Erosion of Surfaces in the Presence of Anomalous Ion Heating in the Plume Region of a High-power Magnetically Shielded Hall Thruster

I. G. Mikellides and A. Lopez Ortega
Jet Propulsion Laboratory, California Institute of Technology

Session 5: Plasma-wall Interactions
 $E \times B$ Plasmas Workshop 2022, Madrid, Spain (online event)
February 16-18, 2022

Plasma-wall Interactions Between the Ion Beam and Cathode Plume of Great Interest in Magnetically Shielded Hall Thrusters

- Magnetic shielding derived more than a decade ago [1,2], eliminated erosion of the discharge channel walls as the driving life-limiting process in Hall thrusters.
- Subsequent tests in a lab thruster (H6MS) revealed small but measurable sputtering along the front magnet pole
 - erosion rates significantly lower than along channel walls of unshielded Hall thrusters and thus of no major risk to long duration missions → NASA develops HERMeS
 - not observed in unshielded thrusters
 - understanding process that led to it would eliminate perceived risks and prolong thruster life even more
- Plasma measurements in this region also revealed
 - broad ion velocity distribution functions measured by LIF (effective ion temperatures several to tens of eV if fitted to Maxwellians) [3-5]
 - classical mechanisms could not explain all measurements [6]



[1] Mikellides, I. G., Katz, I., Hofer, R. R., and Goebel, D. M., de Grys, K., and Mathers, A., "Magnetic Shielding of the Channel Walls in a Hall Plasma Accelerator," *Phys. Plasmas*, 18 (2011).

[2] Mikellides, I. G., Katz, I., Hofer, R. R., and Goebel, D. M., "Magnetic Shielding of Walls from the Unmagnetized Ion Beam in a Hall Thruster," *Appl. Phys. Lett.*, 102 (2013).

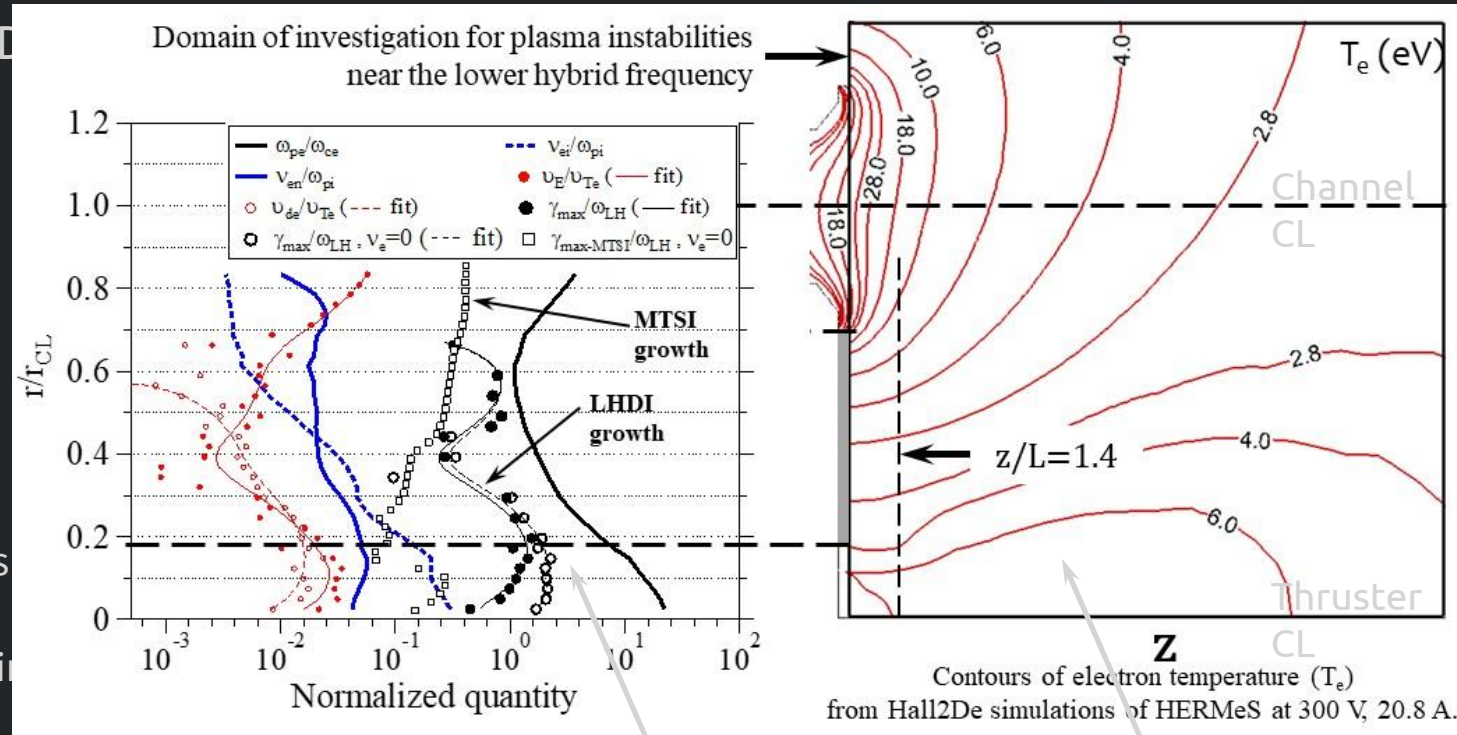
[3] Jorns, B., et al., "Mechanisms for Pole Piece Erosion in a 6-kW Magnetically-Shielded Hall Thruster," AIAA-2016-4839.

[4] Huang, W., Kamhawi, H., "Counterstreaming Ions at the Inner Pole of a Magnetically Shielded Hall Thruster," *J. Appl. Phys.* 129, (2020).

[5] Huang, W., et al., "Ion Velocity Characterization of the 12.5-kW Advanced Electric Propulsion System Engineering Hall Thruster", AIAA-2021-3432

Extensive model validation has revealed a range of physics contributing to the wear of front pole surfaces in magnetically shielded Hall thrusters that were not previously considered.

- Numerical simulations performed using the 2-D axisymmetric hybrid (multifluid/PIC) code Hall2De
- Simulations compared with multiple LIF and wear measurements performed at NASA
- Anomalous effects due to lower hybrid (LH) instabilities [1,2]
 - Enhanced ion heating perpendicular to the magnetic field [3]
 - Isotropization of IVDFs leading to some anomalous heating parallel to the magnetic field
 - Enhanced ion drag (largely in the radial direction) in the otherwise collision-less ion populations
- Sheath and pre-sheath effects
 - Finite sheaths affect largely the wear of the pole cover I/OD edges
 - Pre-sheaths affect largely the flat surfaces facing the plasma plume



From solution to dispersion relations of LH waves [1,2]

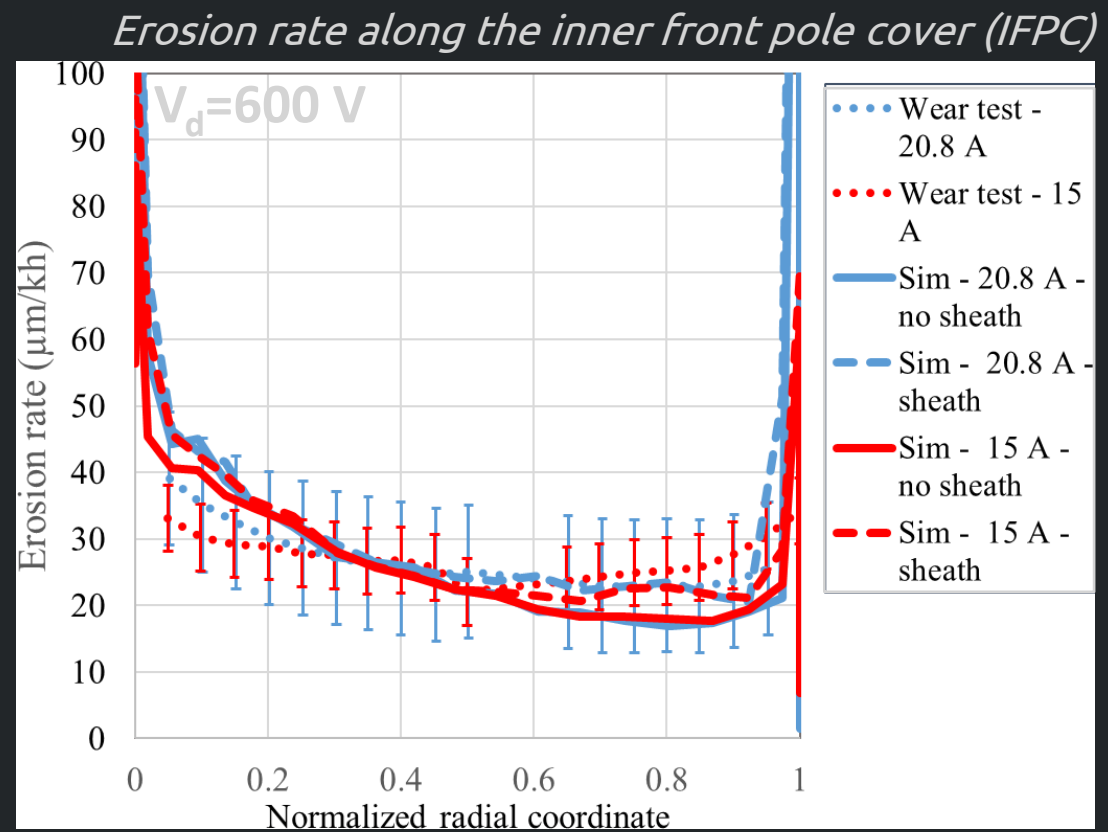
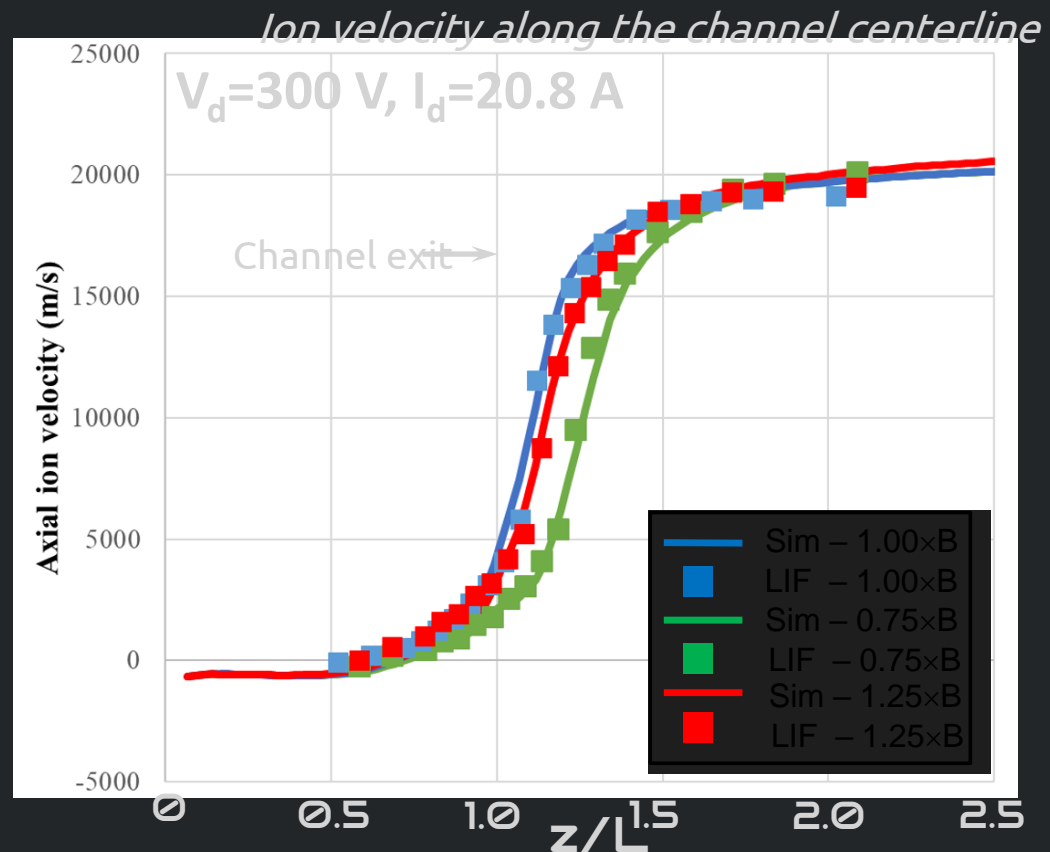
From numerical simulations with Hall2De [3]

[1] Mikellides, I.G. and Lopez Ortega, A., "Growth of the modified two-stream instability in the plume of a magnetically shielded Hall thruster," *Physics of Plasmas*, vol. 27, no. 10, 2020.

[2] Mikellides, I.G. and Lopez Ortega, A., "Growth of the lower hybrid drift instability in the plume of a magnetically shielded Hall thruster," *Journal of Applied Physics*, vol. 129, no. 10, 2021.

Model validation key to identifying and understanding Plasma-wall Interactions in the Front-Pole Plume of Magnetically Shielded Hall Thrusters

- Extensive comparisons between numerical simulations and measurements have been performed to establish the fidelity of the life predictions for the flight version of HERMeS being developed by NASA's industry partner, Aerojet-Rocketdyne, under the Advanced Electric Propulsion System (AEPS) Program.



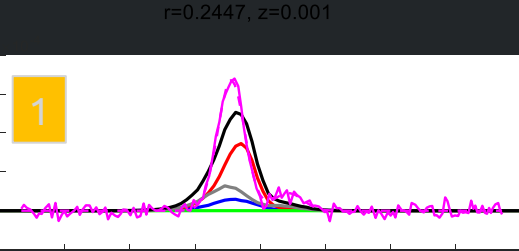
"LIF" = Laser induced Fluorescence measurement
"Sim" = Hall2De simulation

S5: plasma-wall interaction, propellants

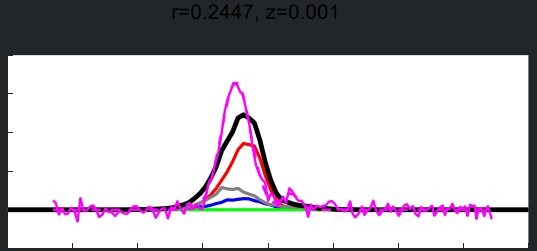
Model validation Key to Identifying and Understanding Plasma-wall Interactions in the Front-Pole Plume of Magnetically Shielded Hall Thrusters

$V_d=600$ V, $I_d=20.8$ A

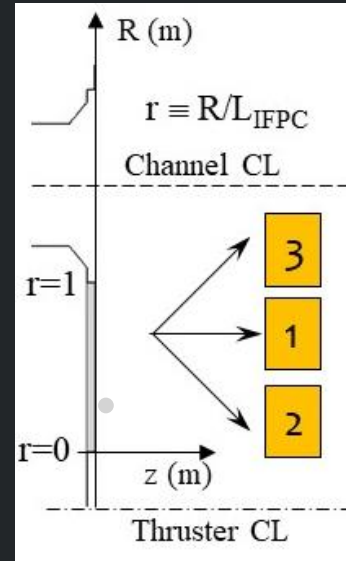
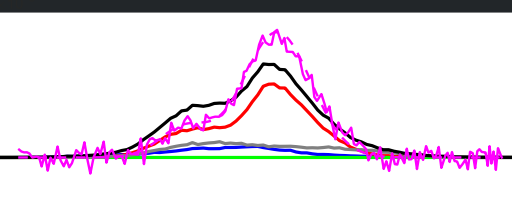
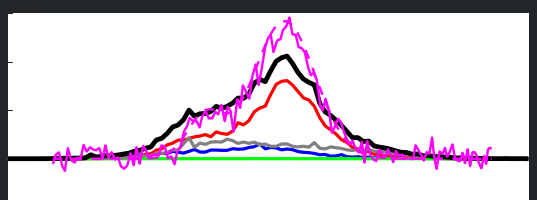
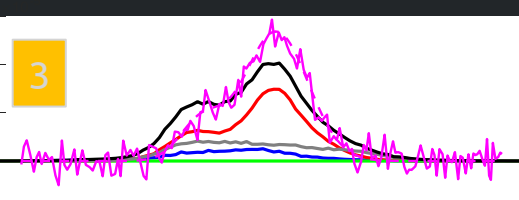
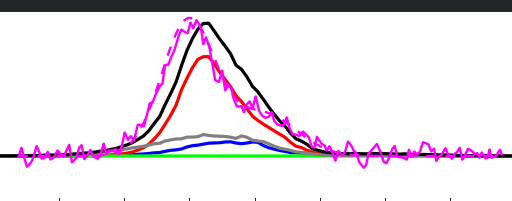
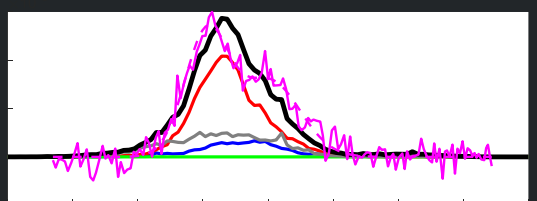
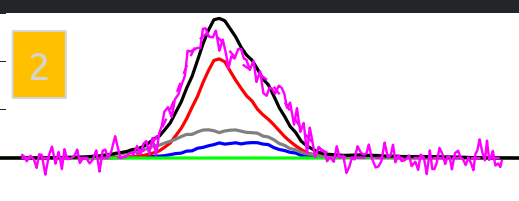
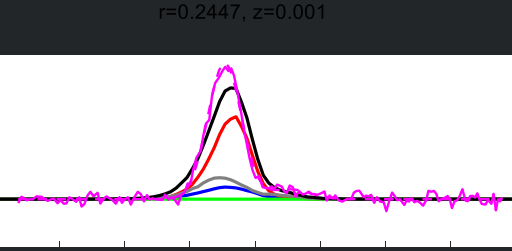
$0.75 \times B$



$1.00 \times B$



$1.25 \times B$



- | |
|---------------------|
| Sim - All ions |
| Sim - Plume Xe+ |
| Sim - Cathode Xe+ |
| Sim - Beam Xe+ |
| Sim - Reflected Xe+ |
| LIF |

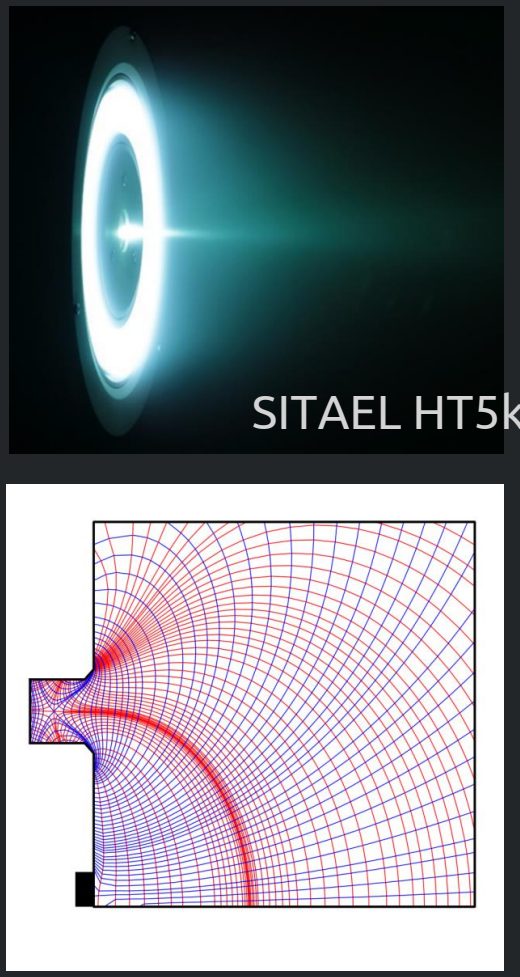
38

"LIF" = Laser induced
Fluorescence measurement
"Sim" = Hall2De simulation

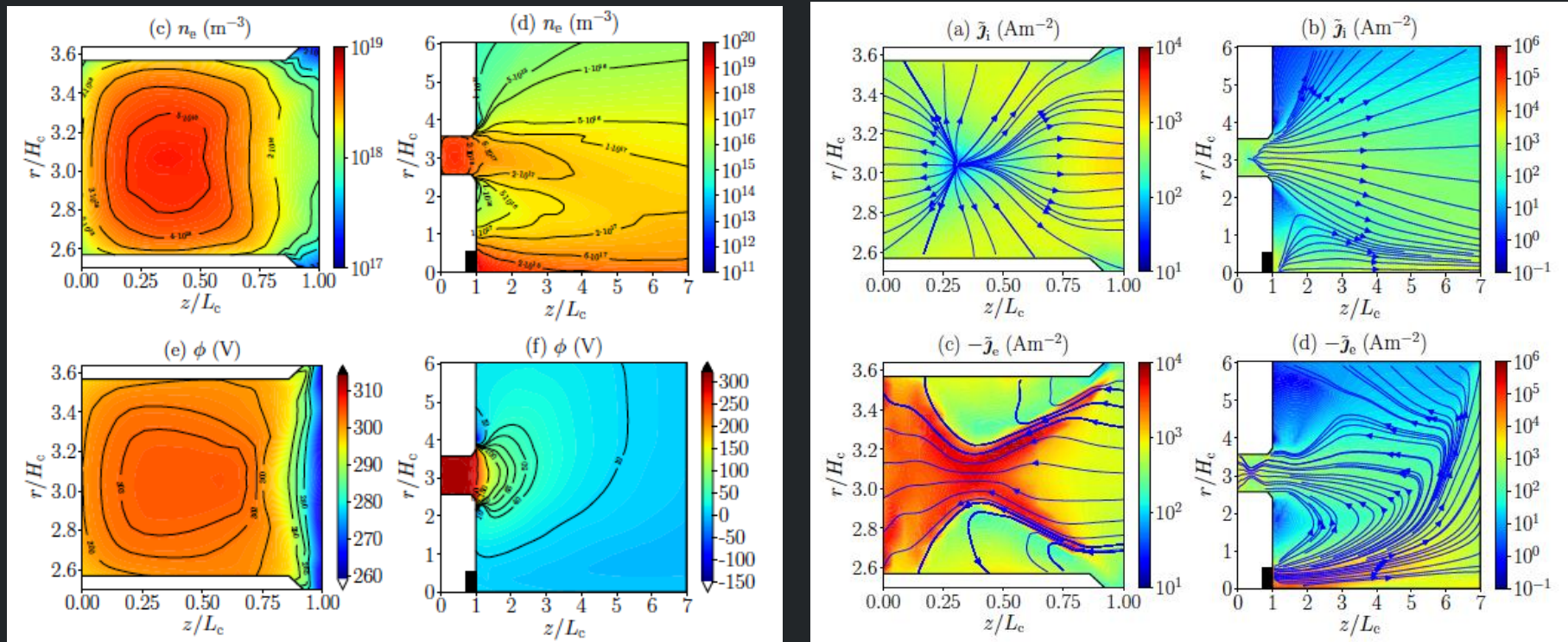
J. Perales et al.

Plasma-wall simulations in MS-HETs

Perales et al.: Simulating plasma-wall interaction in MS-HETs

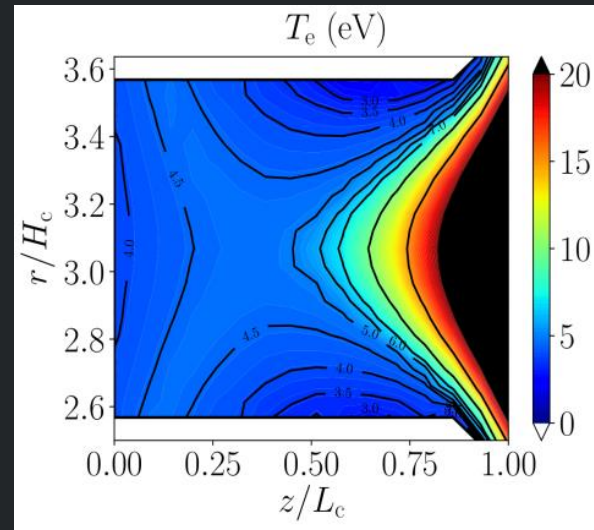


HYPHEN MFAM

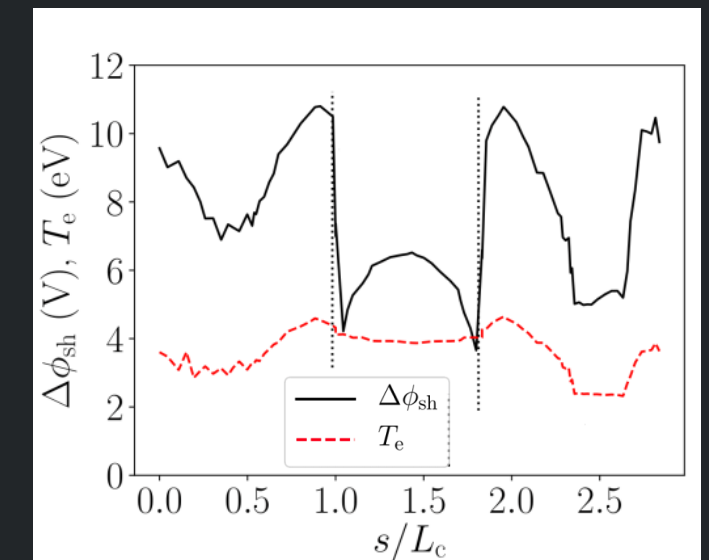
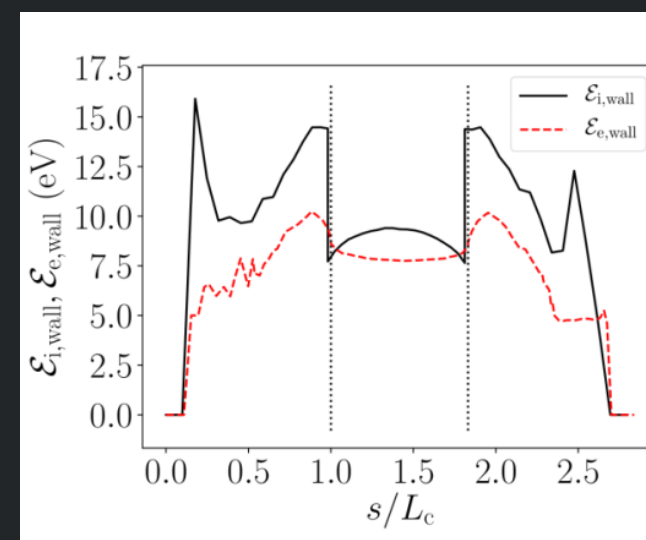
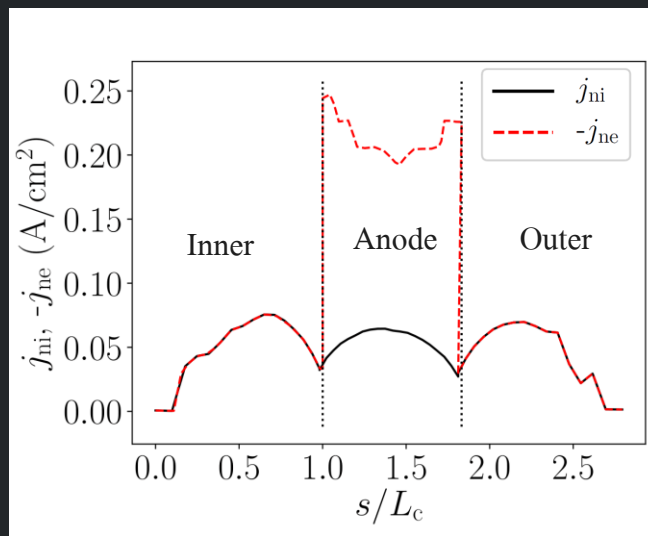


- Acceleration region is outside chamber
- Large plasma density inside chamber
- Electric potential inside is nearly flat and does not follow the B lines, due to ∇p_e
- Central cathode emits electrons and neutrals
 - Electron currents from cathode connect with ion plume and anode

Perales et al.: Simulating plasma-wall in MS-HETs



- Near isothermal magnetic lines
- T_e low inside chamber:
 - Low sheath potential falls
 - Sheaths are conventional → electric field points towards wall
 - Except around chamfers?
 - Low impact energy of ions and electrons:
 - low power losses
 - no erosion



Perales et al.: Simulating plasma-wall in MS-HETs

- Mass and electric current balance:

$$I_{\text{prod}} = I_{i\infty} + I_{iD} + I_{iA} + I_{iC},$$

$$\eta_u = \frac{\dot{m}_{i\infty}}{\dot{m}}, \quad \eta_{\text{cur}} = \frac{I_{i\infty}}{I_d}, \quad \eta_{\text{ch}} = \frac{e\dot{m}_{i\infty}}{m_i I_{i\infty}},$$

Case	V_s (V)	\dot{m}_A (mg/s)	I_{prod} (A)	$I_{i\infty}/I_{\text{prod}}$	I_{iD}/I_{prod}	I_{iA}/I_{prod}	η_u	η_{cur}
1	300	14	27.6	0.42	0.39	0.18	0.94	0.77
2	400	14	33.0	0.36	0.42	0.21	0.94	0.78
3	300	10	17.4	0.45	0.37	0.17	0.91	0.79
4	350	10	18.6	0.42	0.38	0.19	0.90	0.79
5	400	10	18.1	0.44	0.37	0.18	0.92	0.85

- Mass and electric current balance:

$$P = P_\infty + P_D + P_A + P_{\text{inel}},$$

$$\eta_{\text{ene}} = \frac{P_\infty}{P}, \quad \eta_{\text{div}} = \frac{P_{z\infty}}{P_\infty}, \quad \eta_{\text{disp}} = \frac{F^2}{2\dot{m}P_{z\infty}},$$

Case	V_s (V)	\dot{m}_A (mg/s)	P (kW)	η	P_{inel}/P	P_D/P	P_A/P	P_∞/P (= η_{ene})	η_{div}	η_{disp}
1	300	14	4.43	0.57	0.15	0.07	0.05	0.74	0.89	0.87
2	350	14	5.73	0.57	0.13	0.07	0.04	0.74	0.86	0.90
3	300	10	2.91	0.56	0.14	0.06	0.05	0.74	0.88	0.85
4	350	10	3.40	0.56	0.13	0.06	0.05	0.75	0.85	0.88
5	400	10	3.76	0.57	0.11	0.05	0.04	0.78	0.84	0.86

- Comparison with unshielded HETs

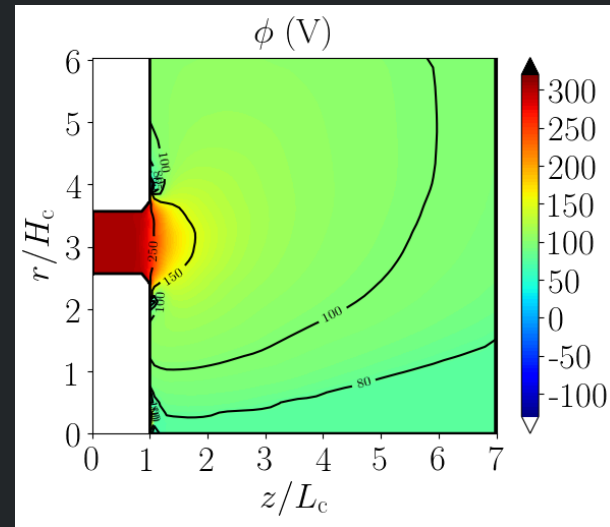
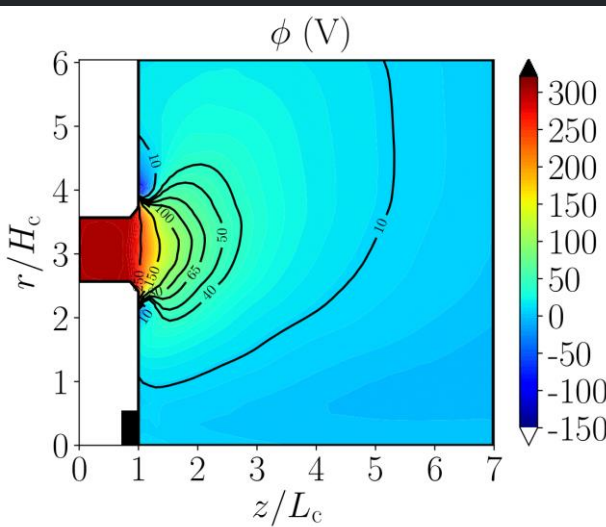
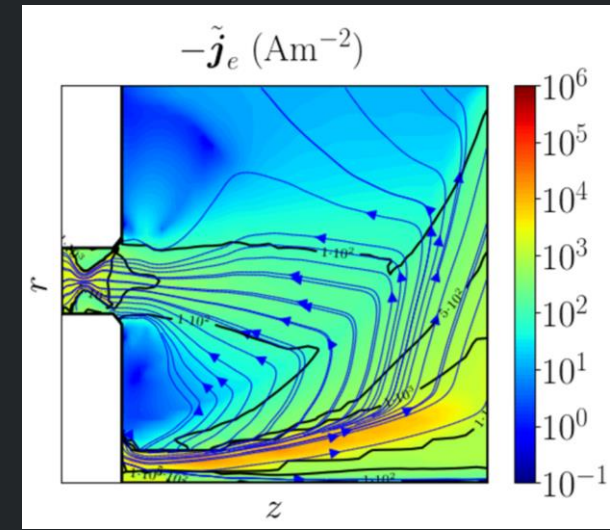
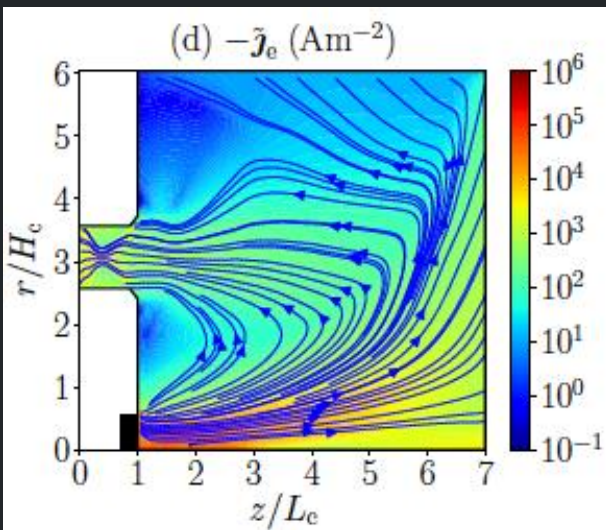
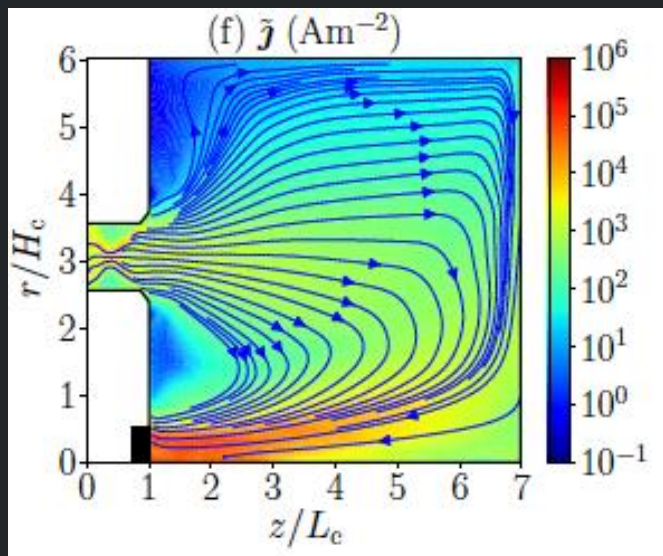
- Similar particle fluxes to chamber lateral walls: lower temperature but higher plasma density
- Larger fluxes to anode
- Much lower energy losses
- Erosion in chamber seems negligible

Perales et al.: Simulating plasma-wall in MS-HETs

Aspects under investigation

(beyond anomalous transport ‘tailoring’)

- Central cathode: electrical bridge with ion plume much facilitated by neutral emission
- Simulation of far (weakly-collisional) plume:
 - Effects of finite plume size and residual magnetic field?
 - Downstream BCs: local vs. global ?



Cathode with neutral emission Cathode without neutral emission

T. Andreussi

MS-HET scaling laws

Andreussi, MS-HET scaling laws

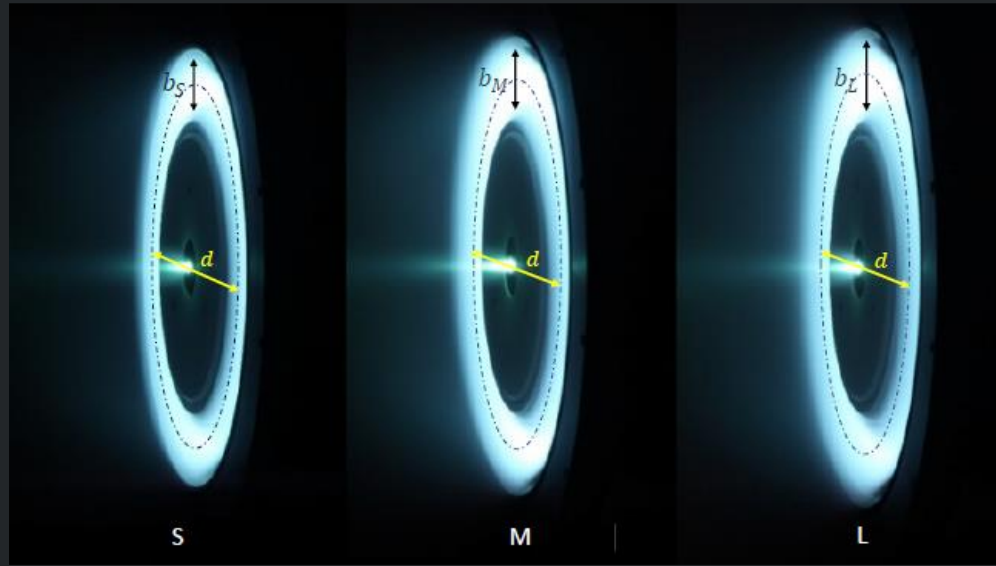
- SITAEL's HT20k DM2 was designed to investigate scaling laws for high-power MS Hall thrusters (20 kW-class)
- Three different channel sizes were tested over a wide range of operating conditions and magnetic fields

$$\frac{b_S}{0.865b_M} < b_M < \frac{b_L}{1.135b_M}$$

- For each operating point, thruster performance and the main characteristics of the discharge current were measured
- To analyze the experimental results, we modeled the relation between control parameters \mathbf{x} and test outputs \mathbf{z} as power laws

$$z_i \propto \prod_{j=1}^n x_j^{a_{ij}} \quad \xrightarrow{\text{Log-linearization}} \quad d\mathbf{z} = \begin{bmatrix} a_{11} & \cdots & a_{14} \\ \vdots & \ddots & \vdots \\ a_{41} & \cdots & a_{44} \end{bmatrix} d\mathbf{x}$$

- Least mean square fitting of the matrix coefficients was performed for each operating condition

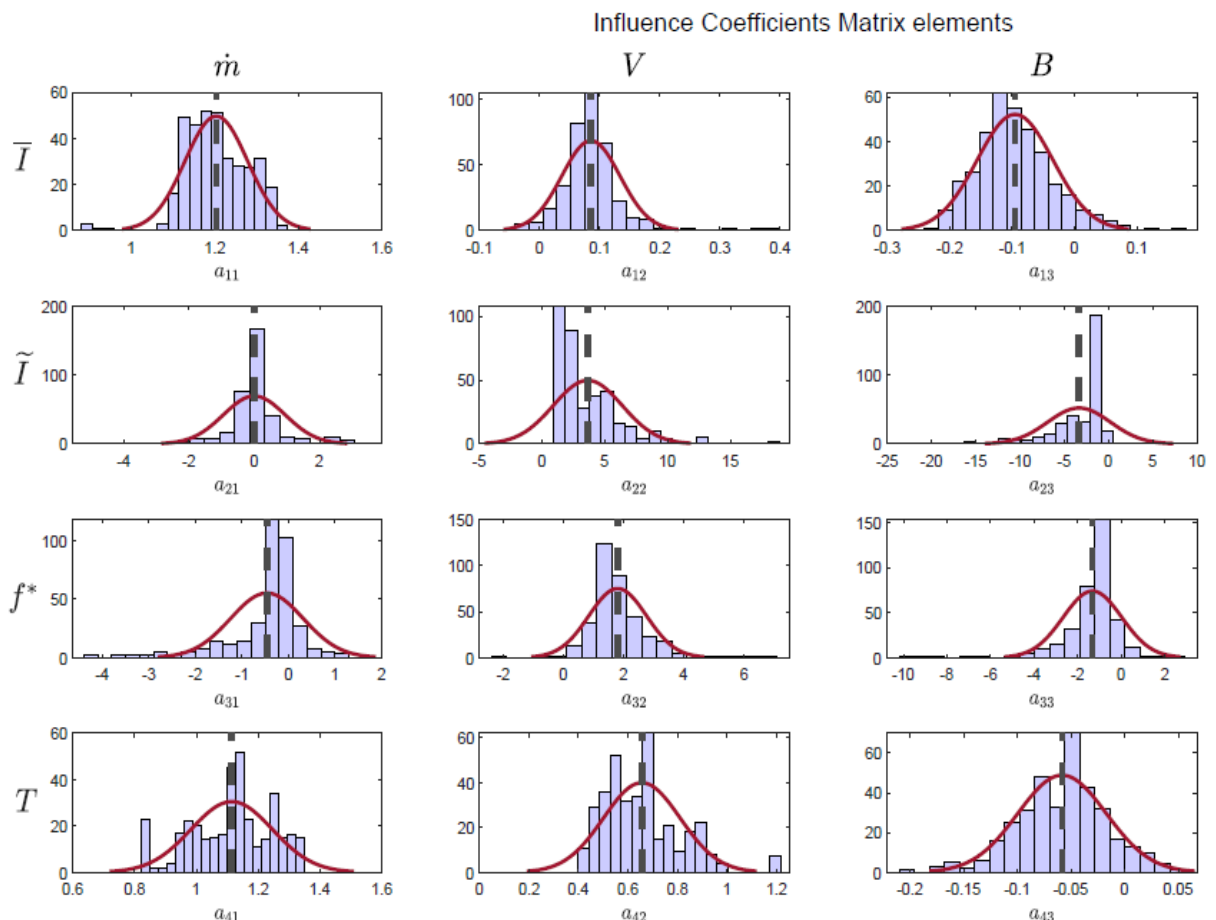


$$\mathbf{x} = \begin{cases} \dot{m} & \text{mass flow rate} \\ V & \text{discharge voltage} \\ B & \text{magnetic field intensity} \\ A & \text{channel frontal area} \end{cases}$$

$$\mathbf{z} = \begin{cases} \bar{I} & \text{average current} \\ \tilde{I} & \text{current AC RMS} \\ f^* & \text{dominant frequency} \\ T & \text{thrust} \end{cases}$$

Andreussi, MS-HET scaling laws

Probability density function



- Known trends recovered (T vs \dot{m} , V ; I vs \dot{m})
- Non-trivial tradeoff between **stability** and **performance** exists:
 - $B \uparrow \quad \tilde{I} \downarrow$ but $\eta \downarrow$
 - $A \uparrow \quad \tilde{I} \downarrow$ but $\eta \downarrow$
- The **ratio V/B** appears to be the dominant parameter for the thruster oscillatory behaviour
 V/B is linked with the electron velocity in an anomalous diffusion dominated plasma

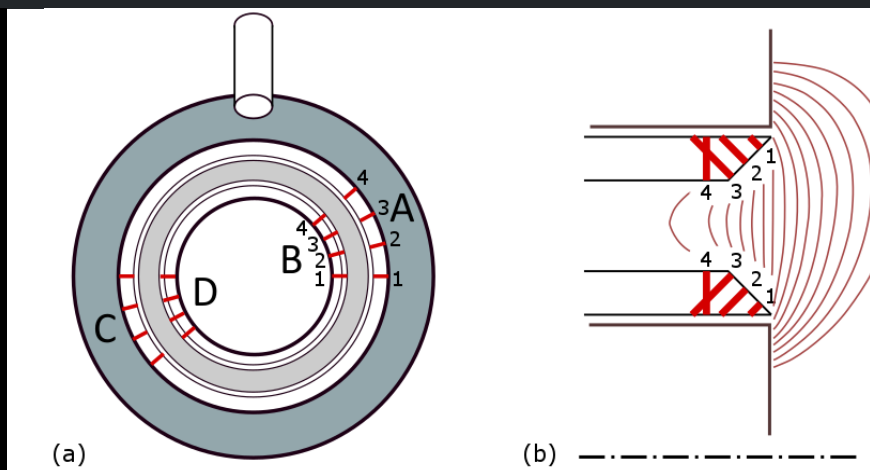
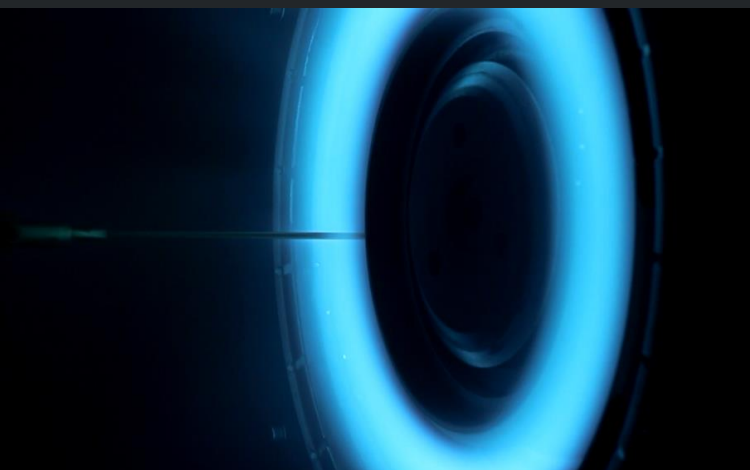
$$|u_e| \propto \frac{V}{B}$$
- \tilde{I} appears to be completely independent from \dot{m} , but it shows a significant dependence on A (at fixed η)
 This suggests that **surface-to-volume ratio** and not density is driving current oscillations

Andreussi, MS-HET Kr vs Xe

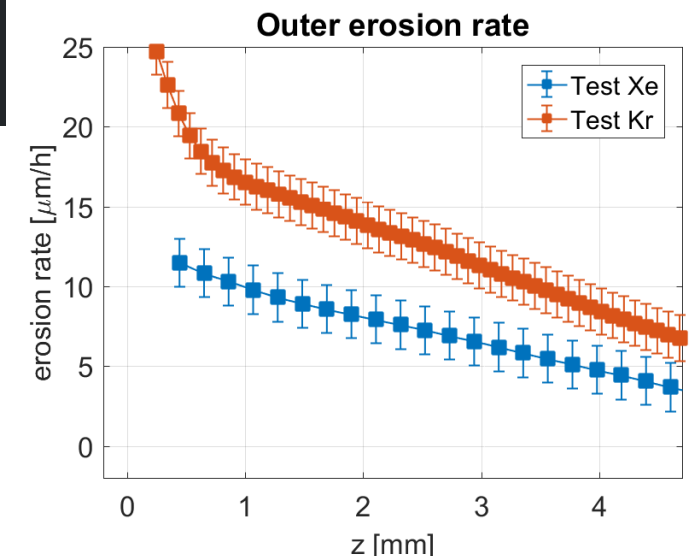
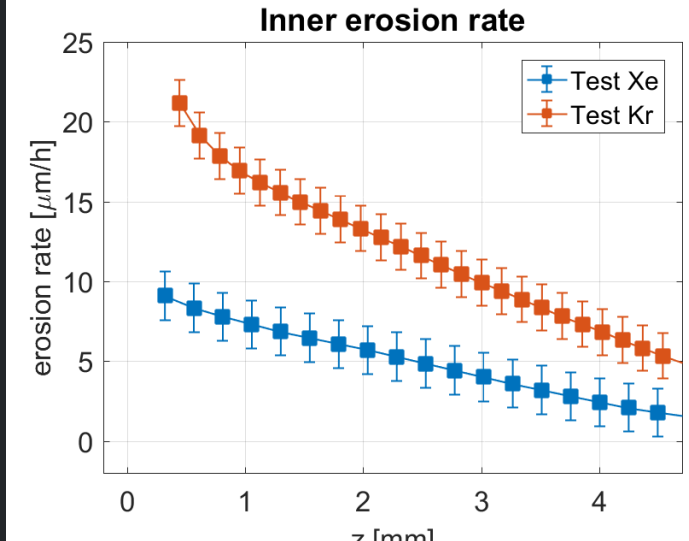
- Due to the interest toward alternative propellants (Krypton), experimental assessment of wall erosion was performed on SITAEL's HT5k
- Wear tests performed on the HT5k DM1 (traditional SPT-like configuration) showed a significant increase of wall sputtering and an estimated total impulse reduction

$$\frac{I_{tot}^{Xe}}{I_{tot}^{Kr}} \sim 2$$

- A new thruster prototype, the HT5k DM2, was assembled to test different configurations (**M1 unshielded, M3 shielded**) and propellants (**Xe vs Kr**)
- Langmuir probes were used to characterize the plasma

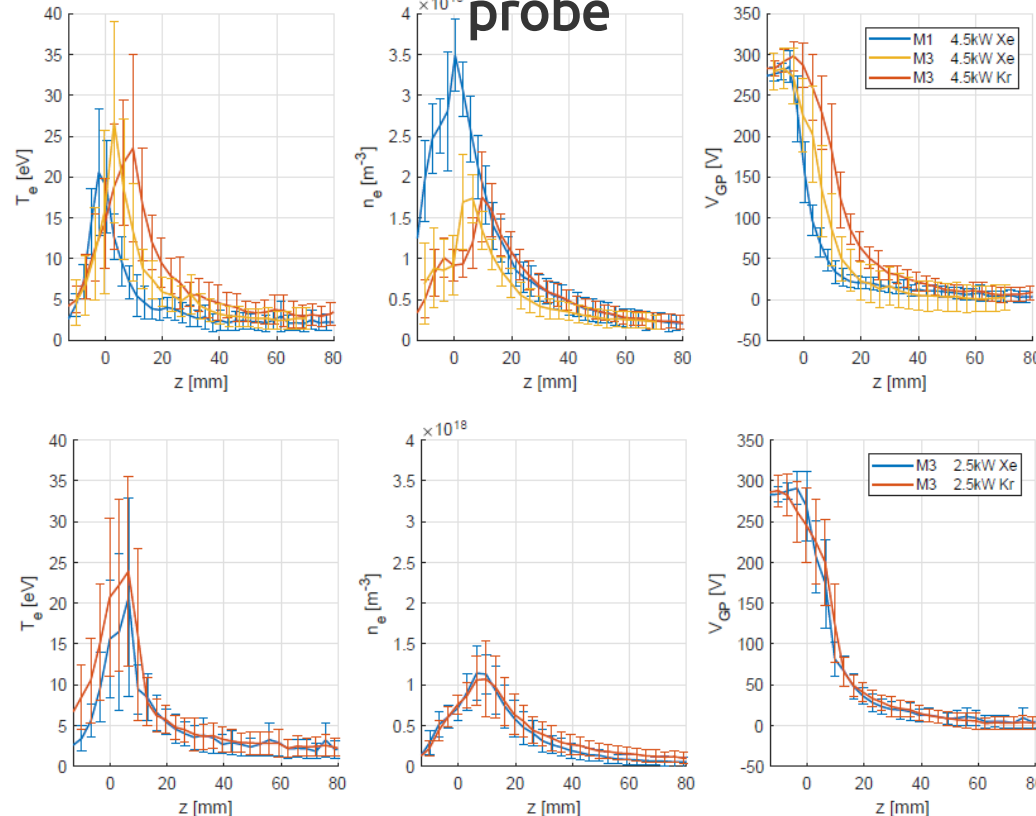


S5: plasma-wall interaction, propellants

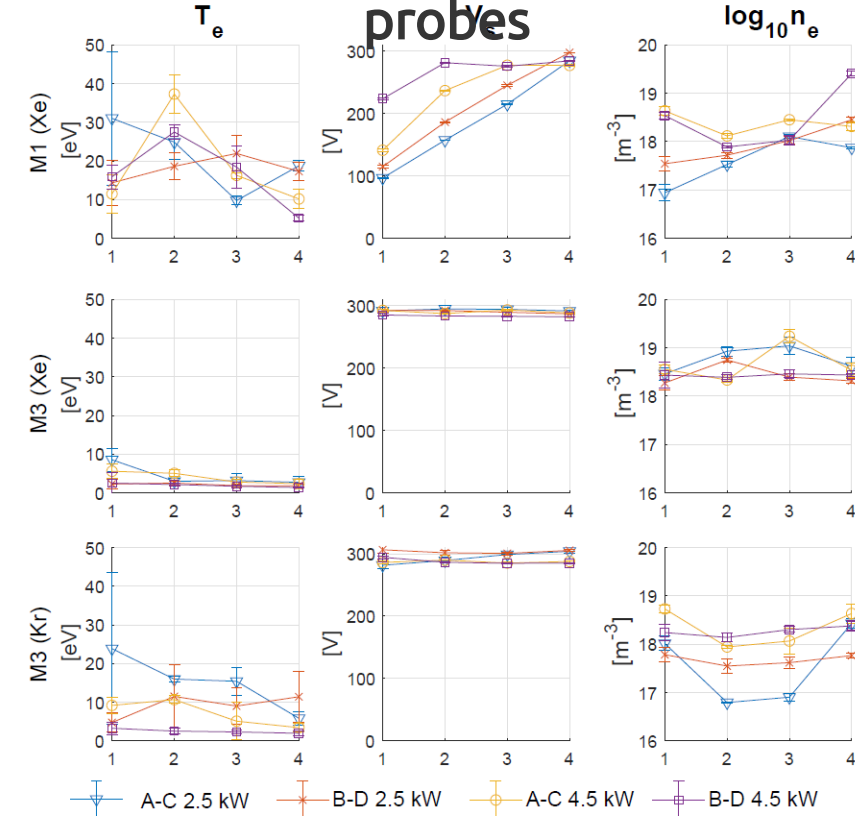


Andreussi, MS-HET Kr vs Xe

Fast-diving triple probe



Flush-mounted single probes

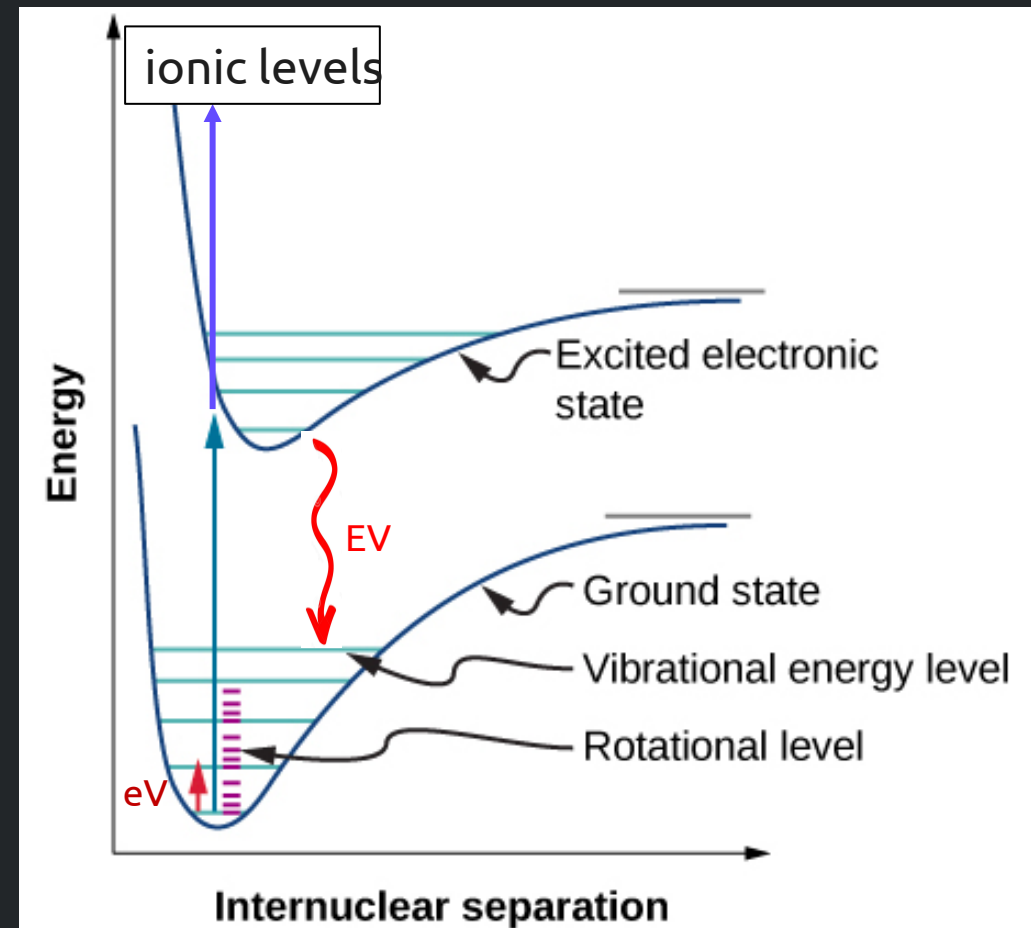


- The electron temperature increases (outside) for the MS configuration, and it is higher for Kr than for Xe.
- Magnetic shielding is effective also for Kr (near-wall potential close to anode potential), but higher electron temperatures are measured inside the channel.

F. Taccogna, J.Zhou,
Molecular Propellant:
data, simulations

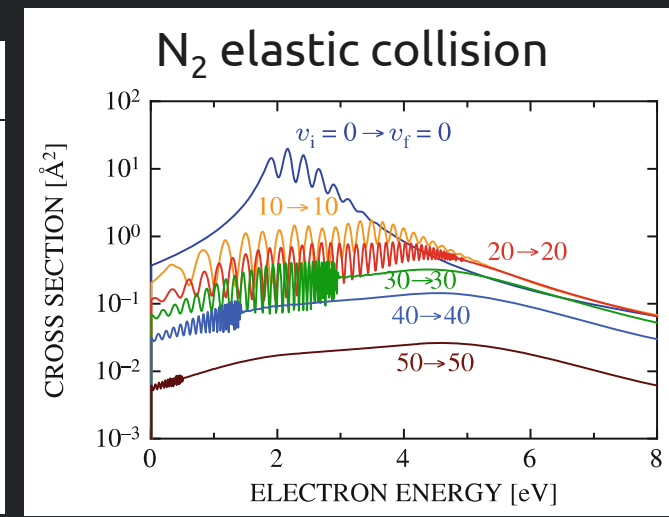
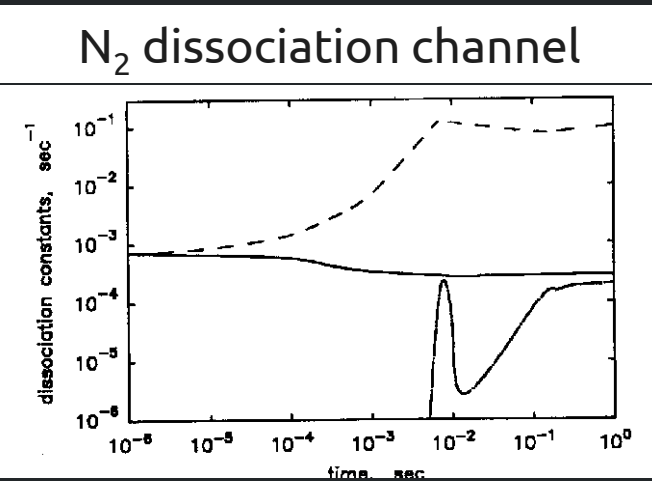
Taccogna-Zhou, Molecular Propellant

- Additional (to electronic excitation “EE” active for atoms) electron power loss channels:
 - rotational excitation “ER” ($E_{th} \approx 10^{-4} - 10^{-2} \text{ eV}$) \rightarrow almost elastic
 - vibrational excitation:
 - direct “eV” transition ($E_{th} \approx 10^{-1} \text{ eV}$) (brown ---)
 - radiative decay from electronic excited states “EV” (green ---)
 - dissociation ($E_{th} \approx 10 \text{ eV}$): excitation to electronic repulsive state
 - dissociative ionization: repulsive molecular ion states
 - dissociative attachment (for electronegative gases)
- Low pressure \rightarrow molecules are always found by electrons in their electronic ground state since spontaneous relaxation by electron dipole radiation is much faster ($\tau_{rad} \approx 10^{-9} \text{ s}$) than the time between collisions (no stepwise ionization);
- Electronic excitations are real losses \rightarrow the electron energy is radiate away (it can pump the vibrational levels of the ground state) \rightarrow ionization from electronic excited states precursors is inefficient (violet ---)



Taccogna-Zhou, Molecular Propellant

- This is not valid for metastable states and their impact needs to be taken into account as additional contributors to ionization
- Electric dipole radiation between vibrational levels of the same electronic state is only permitted for molecules having permanent dipole moments. For the rest (O_2 , N_2 , CO_2), collisional processes can excite strongly nonequilibrium vibrational energy levels contributing to larger dissociation and ionization.
- It is important to self-consistently solve the vibrational kinetic and having vibrational state selective cross sections (see figures →).
- For a polyatomic molecules (H_2O , CO_2) there are many degrees of freedom for vibrational motion, leading to a very complicated vibrational structure.

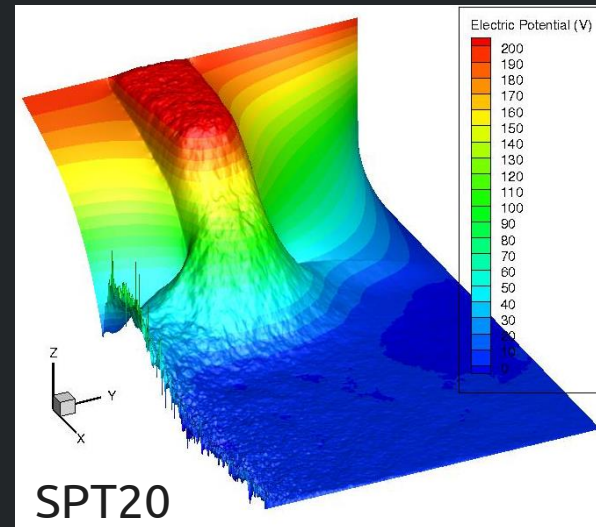


Species	Threshold energy (eV)	Rotational excitation ($J=0 \rightarrow 2$)	Vibrational excitation ($v=0 \rightarrow 1$)	Electronic excitation ($n=1s \rightarrow 2s$)	Dissociation (from $v=0$)	Ionization (from $v=0$)	Dissociative ionization
N	*	*	*	2.39	*	14.54	
O	*	*	*	1.96	*	13.62	
Xe	*	*	*	8.32	*	12.13	
N_2	0.00145	0.29	6.17	9.75	15.58	24.32	
O_2	0.000178	0.19	0.98	5.12	12.06		

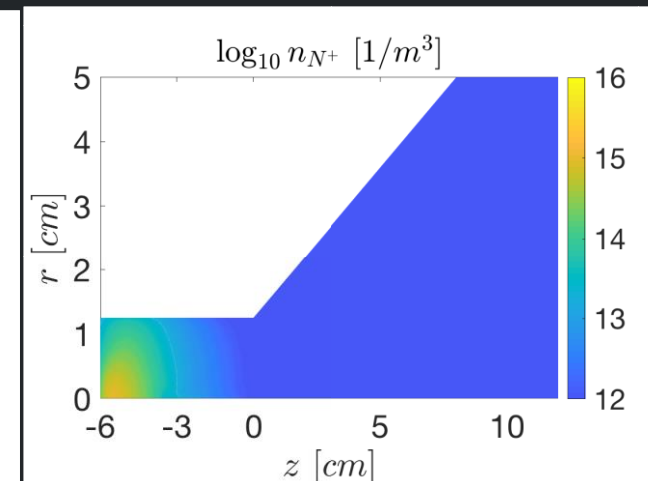
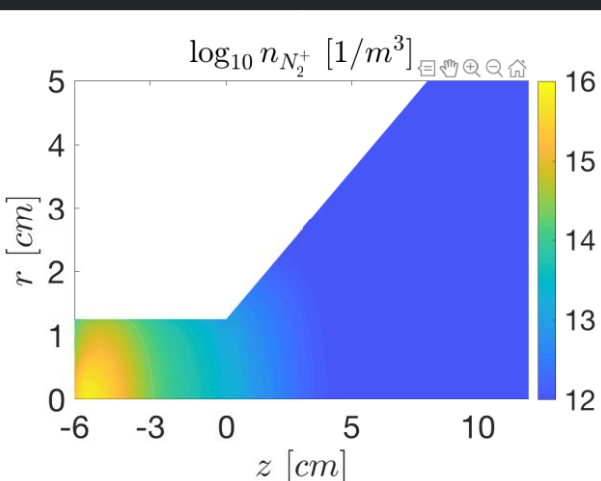
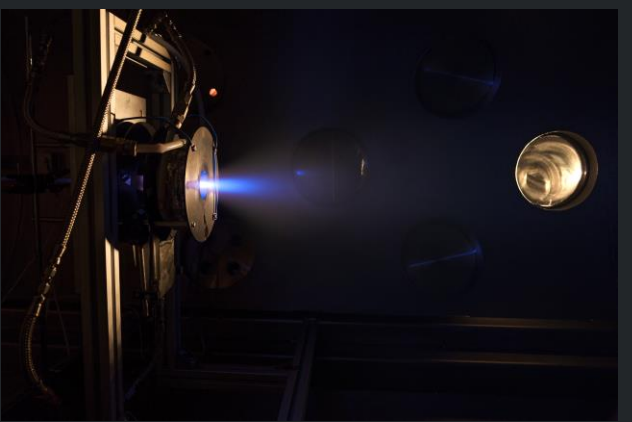
Taccogna-Zhou, Molecular Propellant

Molecular propellant cross-section database implemented in 2 codes

- 2D(r,z) full kinetic PIC-DSMC model «**PICCOLO_2D**»
(CNR-Bari) applied to SPT20



- 2D(r,z) hybrid model «**HYPHEN**»
(UC3M-EP2) applied to an EPT
(similar to HPT05M)



Taccogna-Zhou, Molecular Propellant

Conclusions from PICCOLO_2D applied to SPT20

- As for electronic excitation, also dissociation is mostly a loss channel: atoms produced are faster and formed closer to the exit plane -> less residence time -> bigger (not only longer) discharge channel needed (avoid ion loss on walls)
- In addition, atomic oxygen and nitrogen are very reactive and stick on the wall
- Atomic ion composition is less than 15% and mostly comes from dissociative ionization (75%) rather than from molecular dissociation followed by atomic ionization
- O₂ shows better performances compared to N₂
- Adding atoms (O or even better Xe) helps the performance of pure molecular propellant

Propellant mfr=1 mg/s	Electron power dissipation in eN							Ion composition	Thrust (mN)
	P _{EE,A}	P _{ion,A}	P _{ev,M}	P _{EE,M}	P _{diss}	P _{ion,M}			
Xe	0.45	0.55	*	*	*	*	1:Xe ⁺	1.5	
O ₂	-	-	0.04	0.17	0.16	0.63	0.78:O ₂ ⁺ 0.22:O ⁺	1	
N ₂	0.01	0.1	0.02	0.23	0.23	0.41	0.8:N ₂ ⁺ 0.2:N ⁺	0.7	
Air: N ₂ -O	0.16	0.24		0.15	0.15	0.30	0.4:O ⁺ 0.5:N ₂ ⁺ 0.1:N ⁺	0.8	

Taccogna-Zhou, Molecular Propellant

Conclusions from HYPHEN applied to an EPT

- Tendencies of the plasma chemistry are similar, with some slight differences in the plasma chemistry.
 - Atomic ion composition is still smaller than molecular one, but a bit larger than for SPT20 (until 36%).
 - Power dissipation for atomic species are larger as well, until 27%.
 - Differences may be due to the different plasma production and heating mechanisms.
- Tendencies of overall performances are similar as for SPT20, O₂ better than N₂.

Electron power dissipation in eN								
Propellant mfr=1 mg/s	P _{EE, A}	P _{ion,A}	P _{eV,M}	P _{EE,M} collusion	P _{diss}	P _{ion,M}	Ion composition	Thrust (mN)
Xe	0.4 3	0.57	*	*	*	*	1:Xe ⁺	7.2
O ₂	0.0 8	0.16	0.05	0.21	0.21	0.29	0.66:O ₂ ⁺ 0.34:O ⁺	5.5
N ₂	0.1 6	0.11	0.02	0.39	0.14	0.18	0.64:N ₂ ⁺ 0.36:N ⁺	3.9

D. Rafalskyi

Iodine for space propulsion

D. Rafalskyi, Iodine for space propulsion (1)

Iodine for space propulsion: x9 density (Kr), 100 times cheaper, no high pressure tanks/ no leaks/ filling. First publication dated b

NPT30-I2: first iodine plasma system to be ever tested in space Thrust: 0.4-1.2 mN, Isp: up to 2450 s, Total impulse: up to 5500 Ns

Input power: 35-65 W

Mass/Volume: 1.3 kg, 10x10x10 cm

Smallest ion thruster to be ever flown

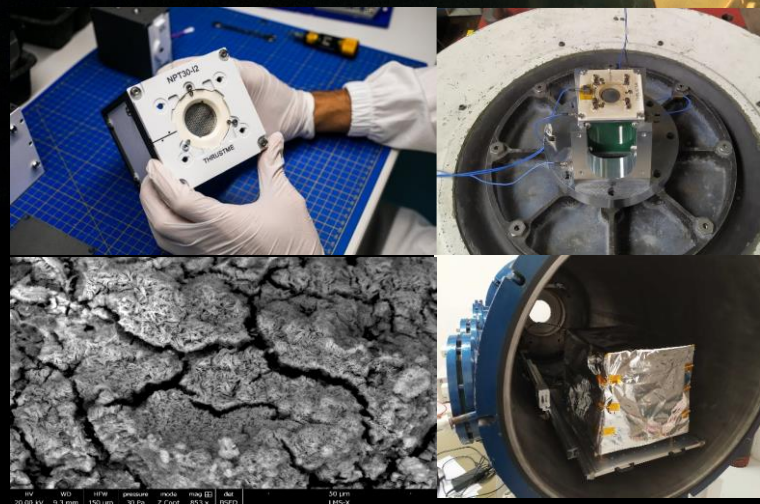
Heavy R&D started at CNRS/Ecole Polytechnique
Development: 2016-2020

Qualifications: (04-06) 2020

Integrated to satellite: 09/2020

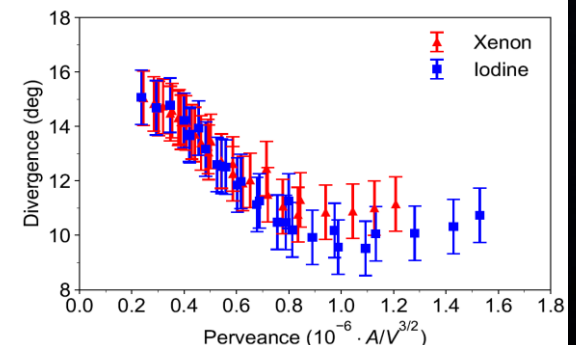
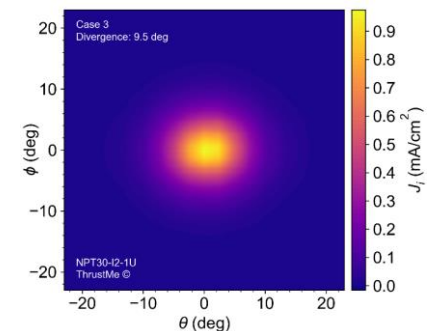
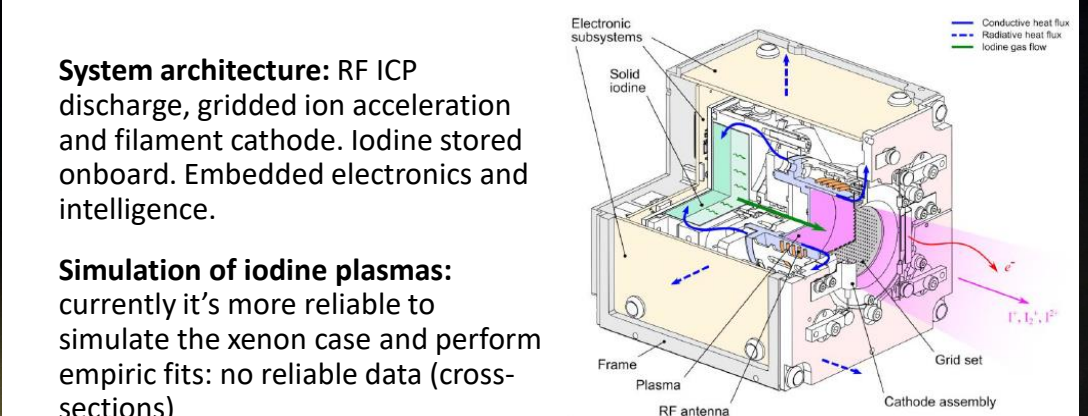
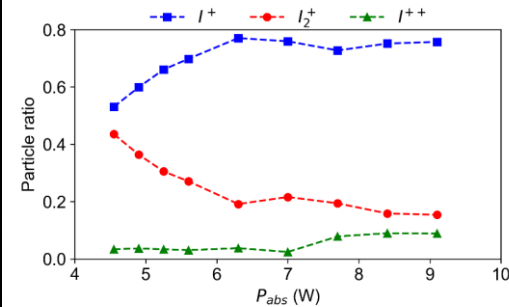
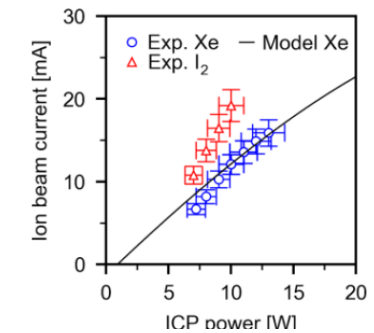
Launched to space: 11/2020

Team of 6 engineers, 3 PhDs and 1 PhD student



System architecture: RF ICP discharge, gridded ion acceleration and filament cathode. Iodine stored onboard. Embedded electronics and intelligence.

Simulation of iodine plasmas: currently it's more reliable to simulate the xenon case and perform empiric fits: no reliable data (cross-sections)



D. Rafalskyi, Iodine for space propulsion (2)

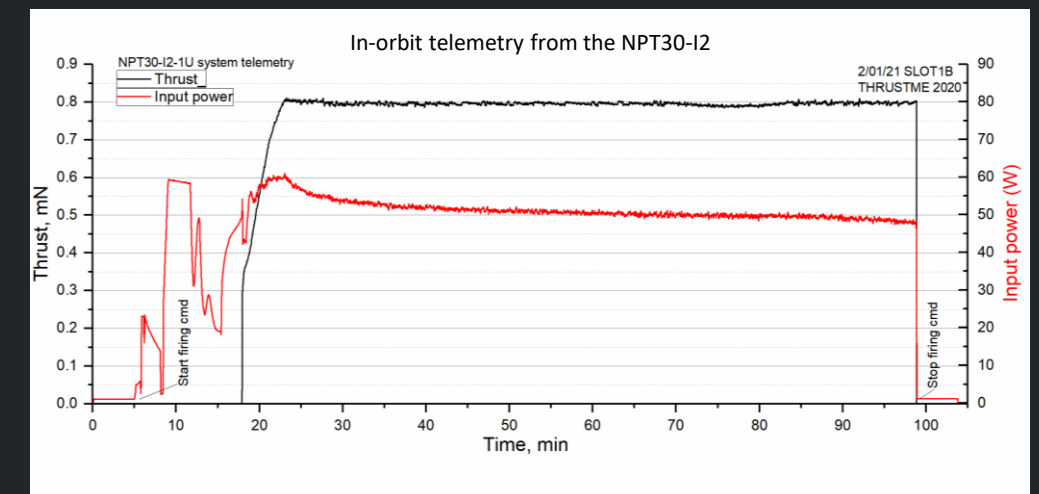
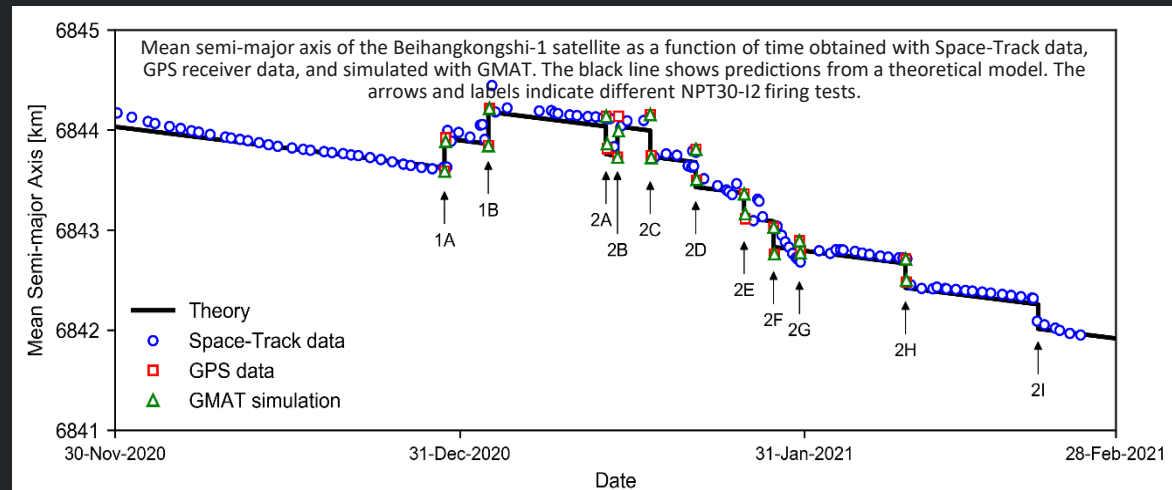
Space flight:

- In-flight performance validated through multiple firings
- Lifetime tests are running in parallel at ThrustMe facility
- Plasma-wall interaction of iodine plume with satellite

materials requires extensive research, no particular effects have been detected in flight yet

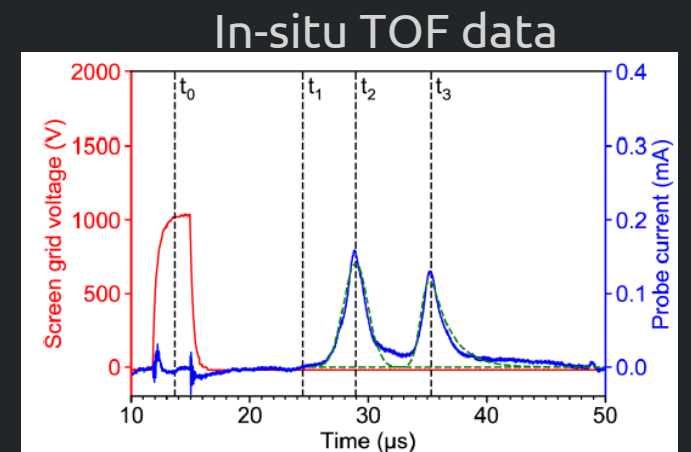
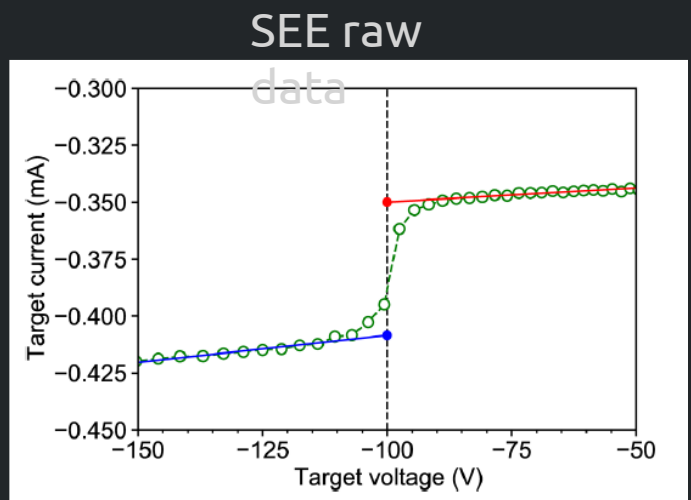
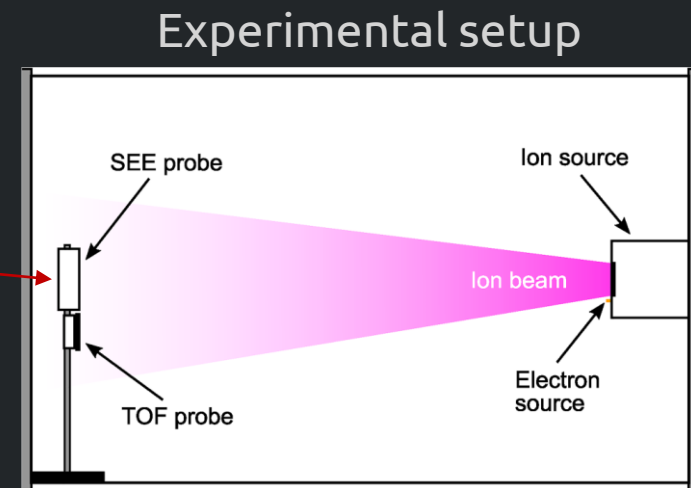
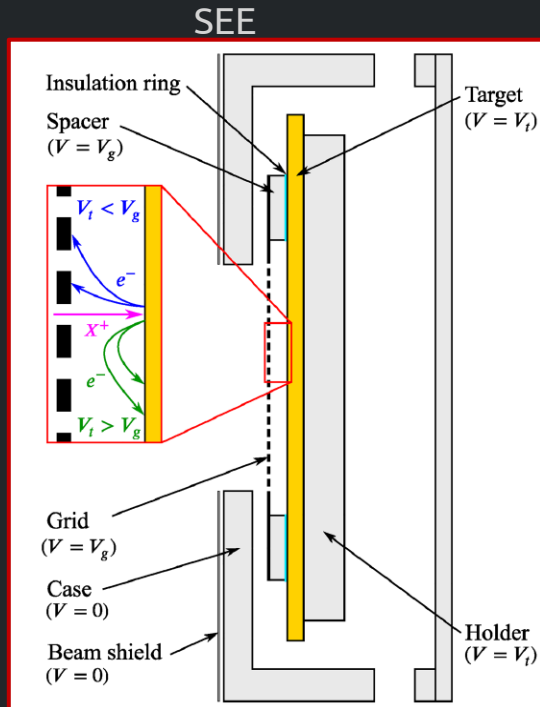
- 5 iodine-fuelled propulsion systems are operated in

space, all produced by ThrustMe; above 20 systems expected by 2022. Continuous telemetry analysis is performed



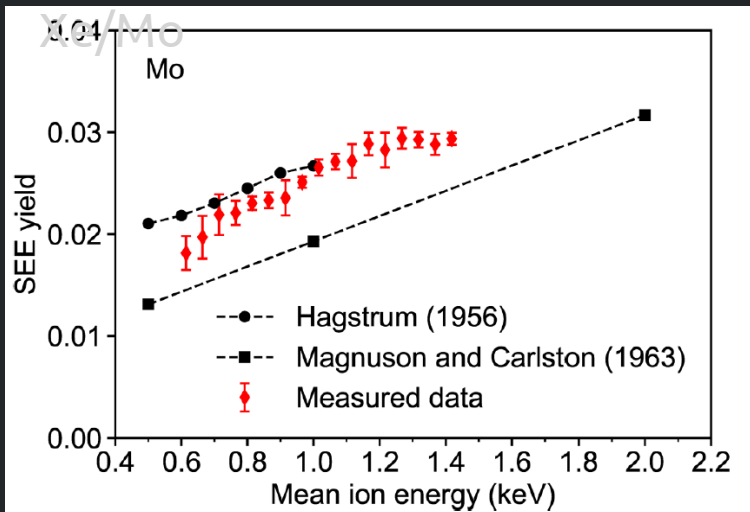
D. Rafalskyi, Iodine for space propulsion (3)

Iodine system development: first SEE measurements for a set of target materials Motivation: no data available for SEE as well as for many basic iodine properties

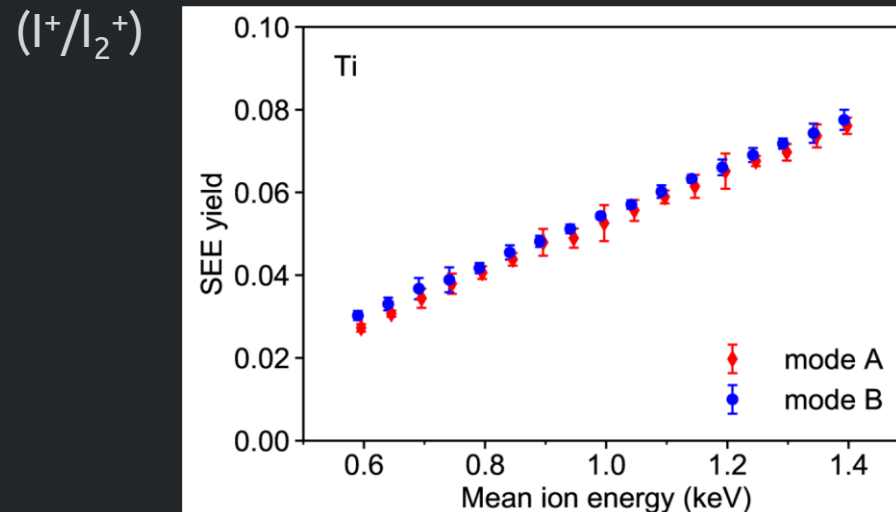


D. Rafalskyi, Iodine for space propulsion (4)

SEE probe validation with



SEE measurements with different ion composition

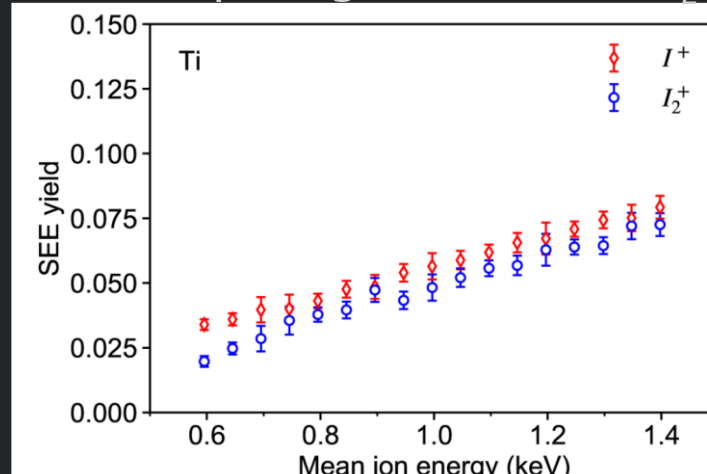


7 target materials studied

Material	Manufacturer	Composition
Molybdenum (Mo)	Goodfellow	Mo > 99.9%
Tungsten (W)	Goodfellow	W > 99.9%
Aluminum (Al)	Goodfellow	Al > 99.0%
Titanium (Ti)	Goodfellow	Ti > 99.6%
Copper (Cu)	Goodfellow	Cu > 99.9%
Carbon–carbon (CC)	Goodfellow	Unspecified
Steel	Precision brand	AISI 1008

Main challenge: chemical reactivity (iodides formation)

Decomposing SEE for I^+ and I_2^+



List of References

List of references

SEE, Ion-wall interaction, Electron VDFs

- T. Tondu, M. Belhaj and V. Inguimbert, J. Appl. Phys. 110, 093301 (2011)
- V. Pigeon, N. Claire, C. Arnas, et al., Phys. Plasmas 27, 043505 (2020)
- J. Roupie, Contribution à l'étude de l'émission électronique sous impact d'électrons de basse énergie ($<=1\text{keV}$) : application à l'aluminium, PhD Thesis Toulouse University, 2013 (in French)
- M. Villemant, Modélisation et caractérisation expérimentale de l'influence de l'émission électronique sur le fonctionnement des propulseurs à courant de Hall, PhD Thesis Toulouse University, 2019 (in French)
- Dominguez et al. 'On heavy particle-wall interaction in axisymmetric plasma discharges', PSST 085004 (2021)
- Marin et al. , 'Macroscopic plasma analysis from 1D-radial kinetic results of a Hall thruster discharge', PSST 115001 (2021)
- Domínguez-Vázquez et al. "Parametric study of the radial plasma-wall interaction in a Hall thruster." Journal of Physics D: Applied Physics 52, 474003 (2019)

List of references

MS HET

- Giannetti V., Piragino A., Paissoni C. A., Ferrato E., Estublier D., Andreussi T., ‘Experimental scaling laws for the discharge oscillations and performance of Hall thrusters’, Journal of Applied Physics 131, p. 013304 (2022). ISSN: 0021-8979. DOI: <https://doi.org/10.1063/5.0070945>
- Andreussi T., Saravia M. M., Andrenucci M., ‘Plasma characterization in Hall thrusters by Langmuir probes’, Journal of Instrumentation 14, p. C05011 (2019). ISSN: 1748-0221. DOI: <https://doi.org/10.1088/1748-0221/14/05/C05011>
- Andreussi T., Giannetti V., Leporini A., Saravia M., Andrenucci M., ‘Influence of the magnetic field configuration on the plasma flow in Hall thrusters’, Plasma Physics and Controlled Fusion 60, p. 014015 (2018). ISSN: 07413335. DOI: <https://doi.org/10.1088/1361-6587/aa8c4d>
- Perales et al. ‘Hybrid plasma simulations of a magnetically shielded Hall thruster’, submitted to JAP

List of references

Propellants

- Andreussi T., Saravia M. M., Ferrato E., Piragino A., Rossodivita A., Andrenucci M., ‘Identification, Evaluation and Testing of Alternative Propellants for Hall Effect Thrusters’, IEPC-2017-380 (2017)
- A. Gurciullo, A. Lucca Fabris, M.A. Cappelli, “Ion plume investigation of a Hall effect thruster operating with Xe/N₂ and Xe/air mixtures”, J. Phys. D: Appl. Phys. 52 (2019) 464003
- F. Marchioni, M.A. Cappelli, “Extended channel Hall thruster for air- breathing electric propulsion”, J. Appl. Phys. 130, 053306 (2021)
- L. Garrigues, “Computational Study of Hall-Effect Thruster with Ambient Atmospheric Gas as Propellant”, J. Prop. Power 28, 344 (2012)
- J. Zhou et al., ‘Performance analysis of alternative propellants for a helicon plasma thruster’, Space Propulsion 2020+1, SP2020 00191
- D. Rafalskyi, J. Martínez Martínez, L. Habl et al. ‘In-orbit demonstration of an iodine electric propulsion system’, Nature 599: 411-415 (2021). DOI: 10.1038/s41586-021-04015-y. [Open Access]
- L. Habl, D. Rafalskyi, and T. Lafleur ‘Secondary electron emission due to multi-species iodine ion bombardment of different target materials’, Journal of Applied Physics 129: 153302 (2021). DOI: 10.1063/5.0048447.